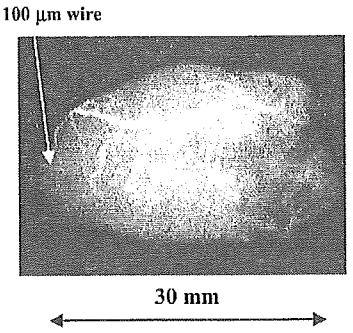

FIG. 12. Angiograms of a rabbit heart. Fine blood vessels of approximately 100 μm were visible.

monochromatic x rays for fluoroscopy can be produced by a similar tube using a constant high-voltage power supply. In conjunction with the fine focusing, these low-cost monochromatic x-ray generators will be employed to perform K-edge angiography and x-ray phase imaging for edge enhancement.[16]

ACKNOWLEDGMENTS

This work was supported by Grants-in-Aid for Scientific Research (13470154, 13877114, and 16591222) and Advanced Medical Scientific Research from MECSST, Grants from Keiryo Research Foundation, The Promotion and Mutual Aid Corporation for the Private School of Japan, JST (Test of Fostering Potential), NEDO, and MHLW (HLSRG, RAMT-nano-001, RHGTEFB-genome-005, and RGCD13C-1).

[a]Electronic mail: dresato@iwate-med.ac.jp

[1]J. J. Rocca, V. Shlyaptsev, F. G. Tomasel, O. D. Cortazar, D. Hartshorn, and J. L. A. Chilla, "Demonstration of a discharge pumped table-top soft x-ray laser," Phys. Rev. Lett. **73**, 2192–2195 (1994).

[2]J. J. Rocca, D. P. Clark, J. L. A. Chilla, and V. N. Shlyaptsev, "Energy extraction and achievement of the saturation linit in a discharge-pumped table-top soft x-ray amplifier," Phys. Rev. Lett. **77**, 1476–1479 (1996).

[3]C. D. Macchietto, B. R. Benware, and J. J. Rocca, "Generation of millijoule-level soft-x-ray laser pulses at a 4-Hz repetition rate in a highly saturated tabletop capillary discharge amplifier," Opt. Lett. **24**, 1115–1117 (1999).

[4]E. Sato, H. Isobe, and F. Hoshino, "High intensity flash x-ray apparatus for biomedical radiography," Rev. Sci. Instrum. **57**, 1399–1408 (1986).

[5]A. Shikoda, E. Sato, M. Sagae, T. Oizumi, Y. Tamakawa, and T. Yanagisawa, "Repetitive flash x-ray generator having a high-durability diode driven by a two-cable-type line pulser," Rev. Sci. Instrum. **65**, 850–856 (1994).

[6]E. Sato, K. Takahashi, M. Sagae, S. Kimura, T. Oizumi, Y. Hayasi, Y. Tamakawa, and T. Yanagisawa, "Sub-kilohertz flash x-ray generator utilizing a glass-enclosed cold-cathode triode," Med. Biol. Eng. Comput. **32**, 289–294 (1994).

[7]K. Takahashi, E. Sato, M. Sagae, T. Oizumi, Y. Tamakawa, and T. Yanagisawa, "Fundamental study on a long-duration flash x-ray generator with a surface-discharge triode," Jpn. J. Appl. Phys., Part 1 **33**, 4146–4151 (1994).

[8]E. Sato, K. Takahashi, M. Sagae, S. Kimura, T. Oizumi, Y. Hayasi, Y. Tamakawa, and T. Yanagisawa, "Sub-kilohertz flash x-ray generator utilizing a glass-enclosed cold-cathode triode," Med. Biol. Eng. Comput. **32**, 289–294 (1994).

[9]E. Sato, R. Germer, Y. Hayasi, E. Tanaka, H. Mori, T. Kawai, T. Usuki, K. Sato, H. Obara, M. Zuguchi, T. Ichimaru, H. Ojima, K. Takayama, and H. Ido, "Plasma flash x-ray generator (PFXG-02)," Proc. SPIE **4948**, 604–609 (2002).

[10]E. Sato, Y. Hayasi, R. Germer, E. Tanaka, H. Mori, T. Kwai, T. Ichimaru, K. Takayama, and Hideaki Ido, "Quasi-monochromatic flash x-ray generator utilizing weakly ionized linear copper plasma," Rev. Sci. Instrum. **74**, 5236–5240 (2003).

[11]E. Sato, Y. Hayasi, R. Germer, E. Tanaka, H. Mori, T. Kawai, H. Obara, T. Ichimaru, K. Takayama, and H. Ido, "Irradiation of intense characteristic x-rays from weakly ionized linear molybdenum plasma," Jpn. J. Med. Phys. **23**, 123–131 (2003).

[12]E. Sato, Y. Hayasi, R. Germer, E. Tanaka, H. Mori, T. Kawai, H. Obara, T. Ichimaru, K. Takayama, and H. Ido, "Intense characteristic x-ray irradiation from weakly ionized linear plasma and applications," Jpn. J. Med. Imag. Inform. Sci. **20**, 148–155 (2003).

[13]A. Mattsson, "Some characteristics of a 600 kV flash x-ray tube," Phys. Scr. **5**, 99–102 (1972).

[14]R. Germer, "X-ray flash techniques," J. Phys. E **12**, 336–350 (1979).

[15]E. Sato, K. Sato, and Y. Tamakawa, "Film-less computed radiography system for high-speed imaging," Ann. Rep. Iwate Med. Univ. Sch. Lib. Arts Sci. **35**, 13–23 (2000).

[16]A. Ishisaka, H. Ohara, and C. Honda, "A new method of analyzing edge effect in phase contrast imaging with incoherent x-rays," Opt. Rev. **7**, 566–572 (2000).

Japanese Journal of Applied Physics
Vol. 44, No. 1A, 2005, pp. 446–449

Quasi-Monochromatic X-Ray Generator Utilizing Graphite Cathode Diode with Transmission-Type Molybdenum Target

Michiaki SAGAE, Eiichi SATO, Etsuro TANAKA[1], Yasuomi HAYASI, Hidezo MORI[2], Toshiaki KAWAI[3], Toshio ICHIMARU[4], Shigehiro SATO[5], Kazuyoshi TAKAYAMA[6] and Hideaki IDO[7]

Department of Physics, Iwate Medical University, 3-16-1 Honchodori, Morioka 020-0015, Japan
[1]*Department of Nutritional Science, Faculty of Applied Bio-science, Tokyo University of Agriculture, 1-1-1 Sakuragaoka, Setagaya-ku 156-8502, Japan*
[2]*Department of Cardiac Physiology, National Cardiovascular Center Research Institute, 5-7-1 Fujishiro-dai, Suita, Osaka 565-8565, Japan*
[3]*Electron Tube Division #2, Hamamatsu Photonics K.K., 314-5 Shimokanzo, Toyooka Village, Iwata-gun 438-0193, Japan*
[4]*Department of Radiological Technology, School of Health Sciences, Hirosaki University, 66-1 Honcho, Hirosaki 036-8564, Japan*
[5]*Department of Microbiology, School of Medicine, Iwate Medical University, 19-1 Uchimaru, Morioka 020-8505, Japan*
[6]*Shock Wave Research Center, Institute of Fluid Science, Tohoku University, 2-1-1 Katahira, Aoba-ku, Sendai 980-8577, Japan*
[7]*Department of Applied Physics and Informatics, Faculty of Engineering, Tohoku Gakuin University, 1-13-1 Chuo, Tagajo 985-8537, Japan*

(Received June 19, 2004; accepted October 15, 2004; published January 11, 2005)

An X-ray generator consists of a negative high-voltage power supply and a field-emission-type cold-cathode X-ray tube. The tube is a glass-enclosed diode utilizing a transmission-type molybdenum target with a thickness of 20 μm, a needle graphite (carbon) cathode, a glass tube body, and a 0.5-mm-thick beryllium window. The tube current decreases gradually with time. After aging for 30 minutes, the tube current was approximately 0.2 mA with a tube voltage of 25 kV, and the focal-spot dimensions were 2.2 × 1.6 mm. Characteristic X-rays of molybdenum K-series were obtained after penetrating the molybdenum target and the beryllium window, and the K-absorption edge was observed clearly. The generator produced number of K photons was approximately 4×10^6 photons/cm^2·s at 1.0 m from the source. The average photon energies of Kα and Kβ lines were 17.4 and 19.6 keV, respectively, and quasi-monochromatic radiography was performed using a computed radiography system. [DOI: 10.1143/JJAP.44.446]

KEYWORDS: quasi-monochromatic X-rays, characteristic molybdenum X-rays, field emission, transmission target, quasi-monochromatic radiography

1. Introduction

Conventional medical X-ray tubes enable the observation of parts of the inside of the human body that cannot be seen by other ways. The X-ray images obtained with these tubes are exposed by both the bremsstrahlung and characteristic X-rays, unless monochromatic radiography is specifically performed. Monochromatic parallel X-ray beams are produced by synchrotrons using single crystals, and these beams have been employed to perform enhanced K-edge angiography[1–3] and X-ray phase imaging.[4,5] Subsequently, monochromatic X-ray computed tomography at two different energies has provided information on the electron density of human tissue.[6] In addition, a compact pulsed tunable monochromatic X-ray source has been designed, developed, and tested.[7] From the source, conical X-ray beams from 10 to 50 keV with pulse widths of 8 ps have been produced, and these beams are useful for biomedical imaging and protein crystallography.

Currently, flash X-ray generators[8–12] utilize cold-cathode radiation tubes and produce extremely high-dose-rate X-ray pulses with durations of less than 1 μs. In order to produce monochromatic X-rays, plasma flash X-ray generators are useful, since intense and sharp characteristic X-rays have been produced from weakly ionized linear plasmas of nickel,[13] copper[14] and molybdenum,[15] while bremsstrahlung rays are rarely detected.

In order to produce steady-state X-rays using a cold-cathode tube, the combination of the target and cathode electrodes is a very important factor. In view of the cathode, a carbon nanotube[16] is a useful field emitter and can be used as a cold cathode in an X-ray tube. Without using nanotubes, electrons can be emitted comparatively easily when lines of electric force are concentrated on a needle tip. Characteristic K-series X-rays have been obtained using a filter made of the same element as the target.

In the present research, we developed a cold-cathode X-ray tube with a needle-shaped graphite cathode, and applied it to produce characteristic molybdenum K-series X-rays by uisng a transmission target.

2. Generator

Figure 1 shows the block diagram of the X-ray generator, which consists of a negative high-voltage power supply (Model 500, −100 kV-3 mA, Pulse Electric Eng. Inc.) with dimensions of 450 × 430 × 150 mm and an X-ray tube. In the X-ray tube, the negative high voltage is applied to the cathode electrode, and the anode (target) is connected to the ground potential.

The X-ray tube is a cold-cathode diode type, as illustrated in Fig. 2. In order to perform soft radiography, including mammography, we developed a quasi-monochromatic X-ray tube with a molybdenum target. This tube consists of the following major devices: a needle-shaped graphite cathode with a tip angle of 54° and a diameter of 3.0 mm, a

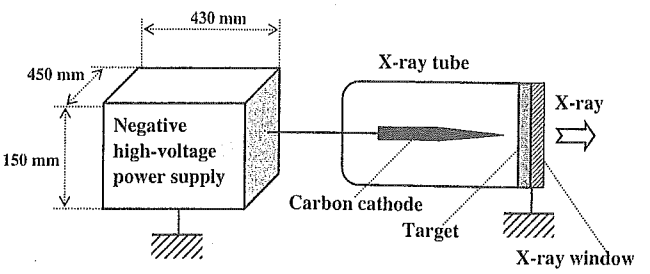

Fig. 1. Block diagram of quasi-monochromatic X-ray generator with cold-cathode diode.

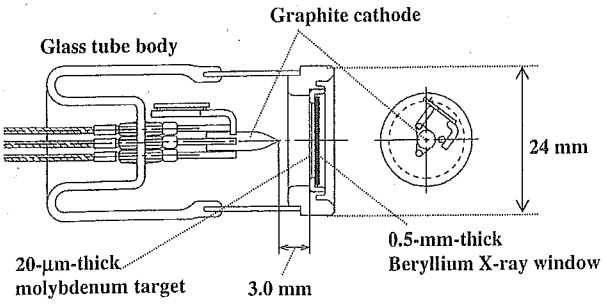

Fig. 2. Structure of X-ray tube.

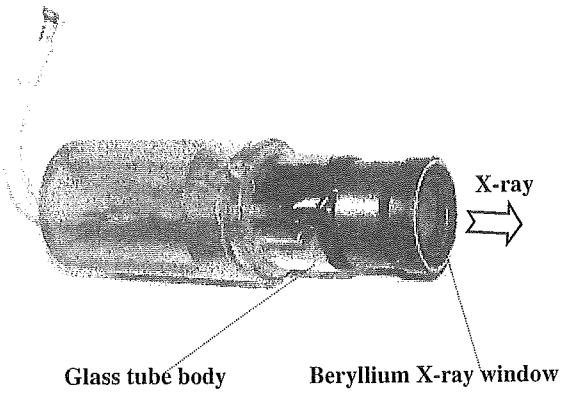

Fig. 3. Cold-cathode X-ray tube with transmission-type molybdenum target.

molybdenum disk target 20 μm thick, and a glass tube body. The target-cathode distance is 3.0 mm, and the transmission X-rays are obtained after the beam passes through the target and a 0.5-mm-thick beryllium X-ray window (Fig. 3). In this case, since the target plays the role of a K-edge filter for effectively absorbing bremsstrahlung X-rays with energies higher than the K-absorption edge, characteristic K-series X-rays are produced. The pressure in the glass-enclosed tube is primarily determined by the pressure when evacuation is stopped, and is approximately 1×10^{-4} Pa. The tube voltage is always constant and is regulated by the constant voltage power supply. Subsequently, the tube current is primarily determined by the tube voltage and the target-cathode distance, and increases with decreasing distance and increasing voltage.

In this experiment, the tube voltage applied was from 20 to 30 kV, and the exposure time was controlled in order to obtain optimum X-ray intensity for radiography.

3. Characteristics

3.1 X-ray intensity

In the field emission X-ray tube, it was very difficult to measure the X-ray intensity correctly, since the intensity gradually decreased during exposure, and small-scale vacuum breakdown may often occur. The X-ray intensity was measured using a Solidose 308 M ionization chamber for mammography at 1.0 m from the X-ray source with an exposure time of 10 s. Because the tube current increased when the tube voltage was increased, the X-ray intensity increased substantially with increasing tube voltage. In this measurement, the intensity rate with a tube voltage of 25 kV was approximately 0.3 μC/kg·s (=10 μJ/kg·s = 10 μGy/s) at 1.0 m from the source.

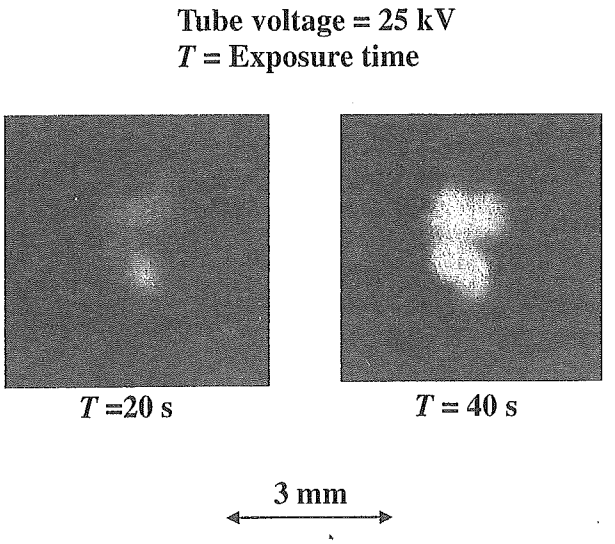

Fig. 4. Images of X-ray source with changes in exposure time.

3.2 X-ray source

In order to measure the images of the X-ray source, we employed a pinhole camera with a hole diameter of 100 μm in conjunction with a Polaroid XR-7 (film). When the exposure time was increased with a tube voltage of 25 kV, the spot intensity increased, but the spot dimensions seldom varied and had values of 2.2 × 1.6 mm (Fig. 4).

3.3 Cathode voltage and tube current

Cathode voltage and tube current were measured using a high-voltage divider and a resistor, respectively (Figs. 5 and 6). In this generator, the cathode voltage is −1 times the tube voltage, and we observed stable cathode voltages. Thereafter, the tube current increased exponentially with increasing tube voltage in a short time. In addition, the current was unstable, and decreased gradually with time.

3.4 X-ray spectra

X-ray spectra were measured using a transmission-type spectrometer with a curved lithium fluoride crystal 0.5 mm thick. The spectra were taken using a computed radiography (CR) system (Konica Regius 150)[17] with a wide dynamic range, and relative X-ray intensity was calculated from Dicom digital data. Figure 7 shows the measured spectra from the transmission-type molybdenum target. We observed lines of characteristic K-series X-rays and K-absorption edges of molybdenum. The characteristic X-ray intensity of the Kα and Kβ lines increased substantially when the tube voltage was increased.

4. Radiography

Radiography was performed using the CR system with a sampling pitch of 87.5 μm. The distance between the X-ray source and the imaging plate was 1.0 m.

Spatial resolution was roughly measured using wires. Radiograms of tungsten wires coiled around a pipe made of polymethyl methacrylate are shown in Fig. 8. Although the

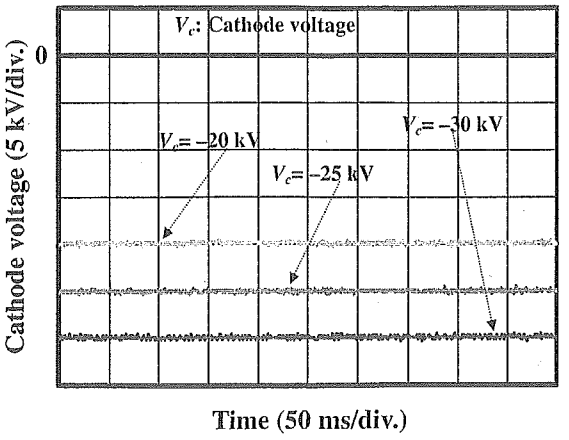

Fig. 5. Cathode voltages.

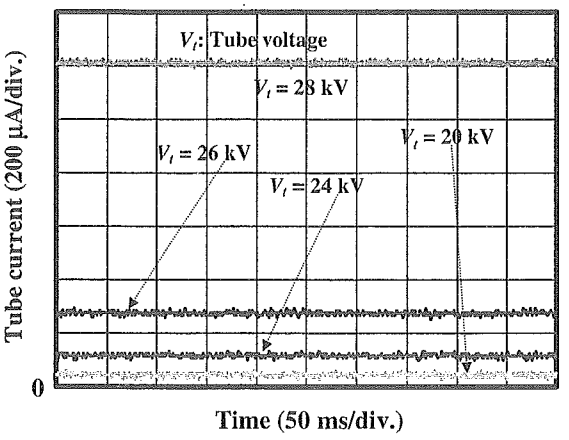

Fig. 6. Tube currents.

image contrast decreased somewhat with decreasing wire diameter due to blurring of the image caused by the sampling pitch, a 50-μm-diameter wire could be observed.

Figures 9 and 10 show angiograms of hearts. Iodine-based microspheres of 15 μm in diameter were used, and coronary

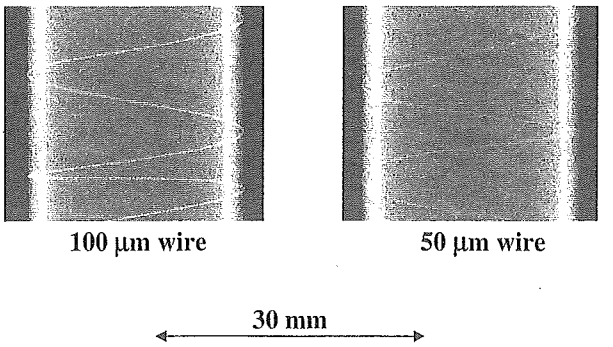

Fig. 8. Radiograms of tungsten wires of 50 and 100 μm diameter coiled around a pipe made of polymethyl methacrylate with tube voltage of 25 kV and exposure time of 20 s.

arteries and fine blood vessels of approximately 100 μm diameter were visible.

5. Discussion

In summary, we developed a simple X-ray generator with the cold-cathode diode and succeeded in producing characteristic molybdenum K-series X-rays using the transmission target as the K-edge filter. Subsequently, we confirmed the filtering effect of the target, and bremsstrahlung X-rays with photon energies higher than the edge were rarely detected with a tube voltage of 23 kV.

The current density J (A/cm^2) under field emission is written as:

$$J = 1.54 \times 10^{-6}(V/d)^2 \cdot \exp(-6.8 \times 10^7 \phi^{1.5} d/V)/\phi, \quad (1)$$

where V (V) is the tube voltage, d (cm) is the target-cathode distance, and ϕ (V) is the work function of the cathode element. Therefore, the current values in Fig. 6 corresponded qualitatively to eq. (1).

During the X-ray exposure, although the tube current decreases slightly due to ion sputtering, stable current flow can be obtained by selecting the appropriate cathode material and by controlling the radius of curvature of the cathode tip. In addition, the generator-produced number of

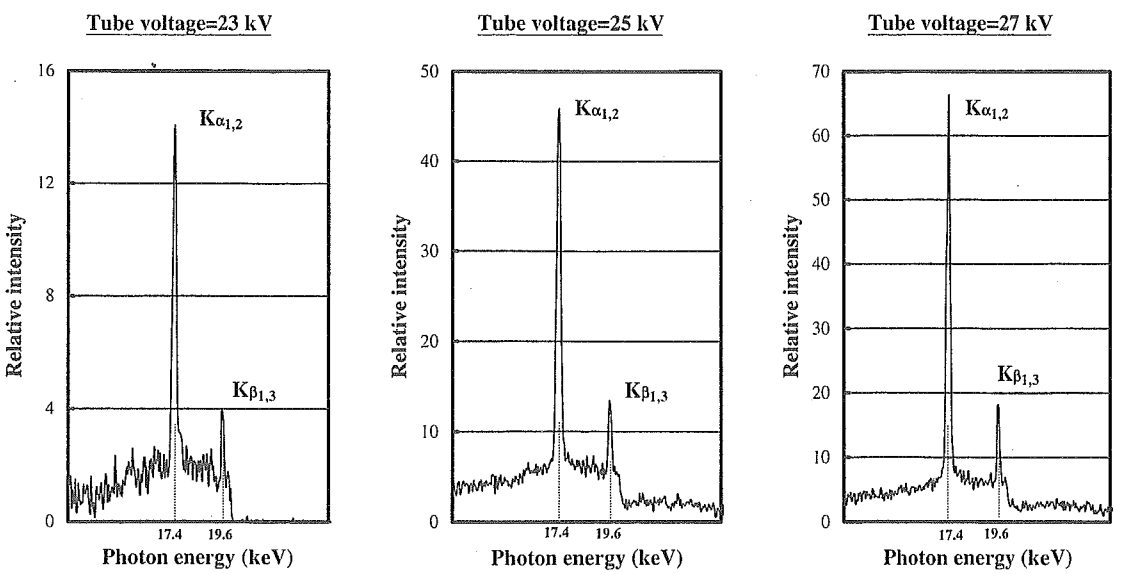

Fig. 7. X-ray spectra.

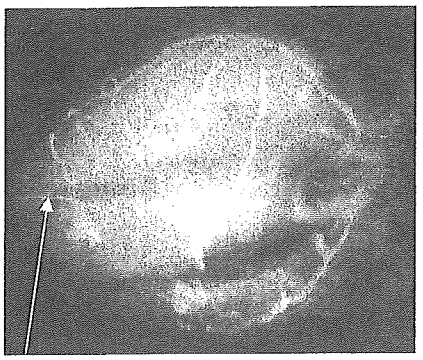

Fig. 9. Angiogram, using iodine microspheres, of extracted rabbit heart. Tube voltage and exposure time were 25 kV and 20 s, respectively.

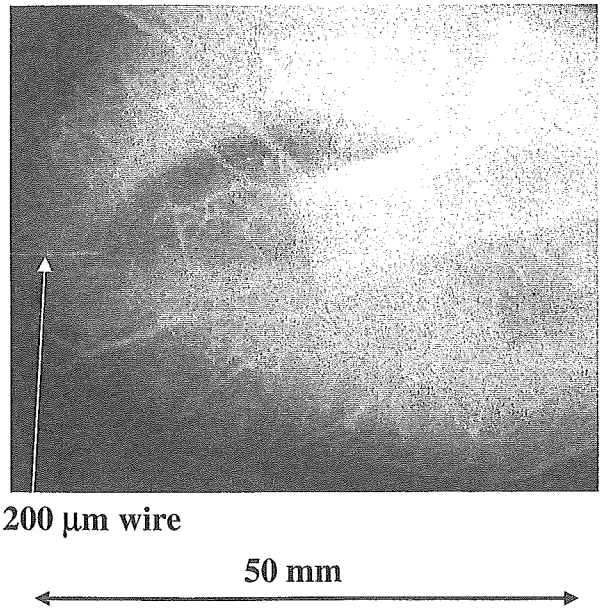

Fig. 10. Angiogram of extracted dog heart with tube voltage of 25 kV and exposure time of 60 s.

characteristic photons was approximately 4×10^6 photons/$cm^2 \cdot s$ at 1.0 m from the source with a tube voltage of 25 kV, and the photon count rate could be increased easily by increasing the tube voltage and current.

The focal spot dimensions decrease with decreasing target-cathode space, and the distance between the X-ray source and the imaging plate should be increased as much as possible to improve the spatial resolution. In soft radiography achieved with characteristic molybdenum K-series X-rays, because an X-ray lens such as a polycapillary plate[18] can be employed, the spatial resolution may be improved by decreasing the inner capillary diameter.

Under the pulsed operation, the high-voltage durability increases substantially, and both the size of the X-ray tube and the diameter of the high-voltage coaxial cable can be decreased. In this case, because the time-average tube current is regulated by the pulse repetition rate, both the tube voltage and the current can be controlled without using a hot cathode.

Recently, we developed a cerium-target X-ray tube to perform enhanced K-edge angiography utilizing cerium Kα rays (34.6 keV), since the rays are absorbed effectively by iodine-based contrast media with a K-edge of 33.2 keV. In addition, Kα rays from ytterbium (52.0 keV), tantalum (57.1 keV), and tungsten (58.9 keV) targets are very useful for performing K-edge angiography using gadolinium-based contrast media with an edge of 50.2 keV. Hence, using these rays, because the absorbed dose can be decreased effectively, extremely low-dose angiography can be accomplished.

Acknowledgment

This work was supported by Grants-in-Aid for Scientific Research (13470154, 13877114, and 16591222) and Advanced Medical Scientific Research from MECSST, Grants from Keiryo Research Foundation, The Promotion and Mutual Aid Corporation for Private Schools of Japan, JST, NEDO, and MHLW (HLSRG, RAMT-nano-001, RHGTEFB-genome-005, and RGCD13C-1).

1) A. C. Thompson, H. D. Zeman, G. S. Brown, J. Morrison, P. Reiser, V. Padmanabahn, L. Ong, S. Green, J. Giacomini, H. Gordon and E. Rubenstein: Rev. Sci. Instrum. **63** (1992) 625.
2) H. Mori *et al.*: Radiology **201** (1996) 173.
3) K. Hyodo, M. Ando, Y. Oku, S. Yamamoto, T. Takeda, Y. Itai, S. Ohtsuka, Y. Sugishita and J. Tada: J. Synchrotron Rad. **5** (1998) 1123.
4) T. J. Davis, D. Gao, T. E. Gureyev, A. W. Stevenson and S. W. Wilkims: Nature **373** (1995) 595.
5) A. Momose, T. Takeda, Y. Itai and K. Hirano: Nature Medicine **2** (1996) 473.
6) M. Torikoshi, T. Tsunoo, M. Sasaki, M. Endo, Y. Noda, T. Kohno, K. Hyodo, K. Uesugi and N. Yagi: Phys. Med. Biol. **48** (2003) 673.
7) F. E. Carroll, M. H. Mendenhall, R. H. Traeger, C. Brau and J. W. Waters: Am. J. Roentgenol. **181** (2003) 1197.
8) R. Germer: J. Phys. E: Sci. Instrum. **12** (1979) 336.
9) E. Sato, H. Isobe and F. Hoshino: Rev. Sci. Instrum. **57** (1986) 1399.
10) A. Shikoda, E. Sato, M. Sagae, T. Oizumi, Y. Tamakawa and T. Yanagisawa: Rev. Sci. Instrum. **65** (1994) 850.
11) K. Takahashi, E. Sato, M. Sagae, T. Oizumi, Y. Tamakawa and T. Yanagisawa: Jpn. J. Appl. Phys. **33** (1994) 4146.
12) E. Sato, K. Takahashi, M. Sagae, S. Kimura, T. Oizumi, Y. Hayasi, Y. Tamakawa and T. Yanagisawa: Med. & Biol. Eng. & Comput. **32** (1994) 289.
13) E. Sato, Y. Hayasi, R. Germer, E. Tanaka, H. Mori, T. Kawai, T. Ichimaru, S. Sato, K. Takayama and H. Ido: J. Electron Spectrosc. & Related Phenom. **137–140** (2004) 713.
14) E. Sato, Y. Hayasi, R. Germer, E. Tanaka, H. Mori, T. Kawai, T. Ichimaru, K. Takayama and H. Ido: Rev. Sci. Instrum. **74** (2003) 5236.
15) E. Sato, Y. Hayasi, R. Germer, E. Tanaka, H. Mori, T. Kawai, H. Obara, T. Ichimaru, K. Takayama and H. Ido: Jpn. J. Med. Phys. **20** (2003) 123.
16) H. Sugie, M. Tanemura, V. Filip, K. Iwata, K. Takahashi and F. Okuyama: Appl. Phys. Lett. **78** (2000) 2578.
17) E. Sato, K. Sato and Y. Tamakawa: Ann. Rep. Iwate Med. Univ. Sch. Lib. Arts Sci. **35** (2000) 13.
18) E. Sato, Y. Hayasi, R. Germer, E. Tanaka, H. Mori, T. Kawai, T. Ichimaru, S. Sato, K. Takayama and H. Ido: J. Electron Spectrosc. Related Phenom. **137–140** (2004) 705.

ELSEVIER

Cardiovascular Research 65 (2005) 334–344

Cardiovascular Research

www.elsevier.com/locate/cardiores

Purified cardiomyocytes from bone marrow mesenchymal stem cells produce stable intracardiac grafts in mice

Naoichiro Hattan[a,1], Haruko Kawaguchi[b,1], Kiyoshi Ando[c], Eriko Kuwabara[a], Jun Fujita[d], Mitsushige Murata[d], Makoto Suematsu[b], Hidezo Mori[a], Keiichi Fukuda[d,*]

[a]*Department of Physiology, Tokai University School of Medicine, Japan*
[b]*Department of Biochemistry and Integrative Medical Biology, Keio University School of Medicine, Tokyo, Japan*
[c]*Department of Hematology and Oncology, Tokai University School of Medicine, Japan*
[d]*Department of Medicine, Division of Cardiology, Keio University School of Medicine, 35 Shinanomachi, Shinjuku-ku, Tokyo 160-8582, Japan*

Received 16 April 2004; received in revised form 4 October 2004; accepted 5 October 2004
Available online 28 October 2004
Time for primary review 21 days

Abstract

Objective: We have previously isolated cardiomyogenic cells from murine bone marrow (CMG cells). Regenerated cardiomyocytes are important candidates for cell transplantation, but as they are stem cell derived, they can be contaminated with various cell types, thereby requiring characterization and purification. Our objectives were to increase the efficiency of cell transplantation and to protect the recipients from possible adverse effects using an efficient and effective purification process as well as to characterize regenerated cardiomyocytes.
Methods: Noncardiomyocytes were eliminated from a mixture of stem-cell-derived cells using a fluorescence-activated cell sorter to specifically isolate CMG cells transfected with a recombinant plasmid containing enhanced green fluorescent protein (EGFP) cDNA under the control of the myosin light chain-2v (MLC-2v) promoter. Gene expression and the action potential were investigated, and purified cells were transplanted into the heart of adult mice.
Results: Six percent to 24% of transfected CMG cells expressed EGFP after differentiation was induced, and a strong EGFP-positive fraction was selected. All the sorted cells began spontaneous beating after 3 weeks. These cells expressed cardiomyocyte-specific genes such as α-skeletal actin, β-myosin heavy chain, MLC-2v, and CaV1.2 and incorporated bromodeoxyuridine for 5 days. The isolated EGFP-positive cells were expanded for 5 days and then transplanted into the left ventricle of adult mouse hearts. The transplanted cells survived for at least 3 months and were oriented in parallel to the cardiomyocytes of the recipient heart.
Conclusions: The purification and transplantation of differentiated cardiomyocytes from adult stem cells provides a viable model of tissue engineering for the treatment of heart failure.

Keywords: Cardiomyocytes; Heart failure; Transplantation; Stem cell; Bone marrow

This article is referred to in the Editorial by B. Dawn and R. Bolli (pages 293–295) in this issue.

1. Introduction

Necrotic cardiomyocytes in infarcted ventricular tissue are progressively replaced by fibroblasts leading to the formation of scar tissue and this loss of cardiomyocytes leads to regional contractile dysfunction. Transplanted fetal cardiomyocytes can survive in heart scar tissue, thereby limiting scar expansion and preventing post-infarction heart failure [1–3]. The transplantation of cultured cardiomyocytes into damaged myocardium has been proposed as a novel method

* Corresponding author. Tel.: +81 3 5363 3874; fax: +81 3 5363 3875.
E-mail address: kfukuda@sc.itc.keio.ac.jp (K. Fukuda).
[1] Naoichiro Hattan and Haruko Kawaguchi contributed equally to this paper.

0008-6363/$ - see front matter
doi:10.1016/j.cardiores.2004.10.004

for treating heart failure. While this is a revolutionary idea, it remains clinically unfeasible due to the difficulty in obtaining donor fetal hearts. For this reason, research has focused on the development of a cardiomyogenic cell line to treat heart failure by transplantation therapy.

Advances in regenerative medicine have enabled the generation of various cell types from embryonic stem (ES) cells or adult stem cells [4,5]. We recently reported the generation of cardiomyocytes from marrow mesenchymal stem cells in vitro (CMG cells) and demonstrated that these cells spontaneously beat, express atrial natriuretic factors, and possess a fetal ventricular cardiomyocyte-like phenotype [6]. We also reported that cardiomyocytes regenerated from marrow mesenchymal stem cells express α_{1A}, α_{1B}, α_{1D}, β_1, and β_2 adrenergic receptors and M_1 and M_2 muscarinic receptors [7]. Stimulation of the α_1 receptors with phenylephrine caused cardiomyocyte hypertrophy, and stimulation of the β receptors with isoproterenol increased the beating rate and contractility of the regenerated cardiomyocytes. These findings demonstrate the suitability of bone-marrow-derived regenerated cardiomyocytes as a candidate for use in cell transplantation therapy.

Purification of regenerated cardiomyocytes is required prior to use for cardiomyocyte transplantation. The population of cardiomyocytes in ES-cell-derived embryoid bodies is less than 10%, and the population of cardiomyocytes in 5-azacytidine-exposed CMG cells is less than 10–30%. To increase the efficiency of transplantation and protect recipients from possible adverse effects, regenerated cardiomyocytes need to be purified from the population of differentiated cell types prior to cell transplantation. Klug [8] and Muller [9] independently reported that embryonic stem-cell-derived cardiomyocytes could be purified using a cardiomyocyte-specific gene promoter–drug-resistant gene expression system. In this study, we purified bone-marrow-derived cardiomyocytes using a recombinant plasmid containing enhanced green fluorescent protein (EGFP) cDNA under the control of the myosin light chain-2v (MLC-2v) promoter. Purified cells were then transplanted into recipient mice hearts and the success of transplantation was analyzed histologically.

2. Methods

All experimental procedures and protocols were approved by the Animal Care and Use Committees of the Keio University, Japan, and the investigation conforms to the Guide for the Care and Use of Laboratory Animals published by the US National Institutes of Health (NIH Publication No. 85–23 revised 1996).

2.1. Preparation of bone marrow-derived regenerated cardiomyocytes

Murine bone-marrow-derived mesenchymal stem cells (CMG cells) were cultured in Iscove's modified Dulbecco's medium (IMDM) supplemented with 20% FBS as previously described [6,7]. The cells were exposed to 3 μmol/l of 5-azacytidine for 24 h to induce cell differentiation [6].

2.2. Construction of myosin light chain 2v-promoted EGFP plasmid

An expression vector, pMLC2v-EGFP, was constructed by cloning a 2.7-kb *Hin*dIII–*Eco*RI fragment of the rat MLC-2v promoter region [10,11] into the *Hin*dIII–*Eco*RI site of pEGFP-1 (Clontech, Palo Alto, CA), so that EGFP would be expressed under the control of MLC-2v promoter (Fig. 1a). This plasmid also contains the neomycin-resistance gene to enable selection of permanently transfected clones. MLC-2v is specifically expressed in ventricular cardiomyocytes.

2.3. Transfection of MLC2v-EGFP expression plasmid and cell selection

The MLC2v-EGFP plasmid was transfected into CMG cells by liposomal transfection. After 24 h when cells are about 20% confluent, a mixture containing 2 μg of plasmid DNA and 4 μl of LT1 TransIT Polyamine Transfection Reagent (Mirus Corporation) in OPTI-MEM (Life Technologies, Gaithersburg, MD) were added to each 35-mm culture dish. After selection with 1000 μg/ml of G418 for 4 weeks, stably transfected colonies derived from single cells were cloned and pooled. EGFP fluorescence was observed under a fluorescence microscope (Olympus TMD300, Tokyo, Japan).

2.4. Flow cytometry and cell sorting

Flow cytometry and sorting of EGFP(+) cells were performed on a FACS Vantage (Becton Dickinson, Cockeysville, MD). Cells were analyzed by light forward and side scatter and for EGFP fluorescence through a 530 nm band pass filter as they traversed the beam of an argon ion laser (488 nm, 100 mW). Nontransfected control cells were used to set the background fluorescence. Cell sorting was performed 3 days after 5-azacytidine exposure at 500 cells/s as EGFP(+) cells displaying fluorescence higher than the background level were observed at this time point.

2.5. Infection of recombinant adenovirus vectors

Replication-deficient recombinant adenovirus vector, pAdex-LacZ, was constructed by cloning LacZ cDNA into the *Swa*I site of pAdex1CAwt as previously described [12]. In this vector, *E. coli* β-galactosidase is expressed under the control of a strong, ubiquitously expressed, promoter-derived from the cytomegalovirus enhancer-chicken β-actin hybrid [13]. On day 3 after seeding, EGFP(+) cells isolated by FACS were incubated

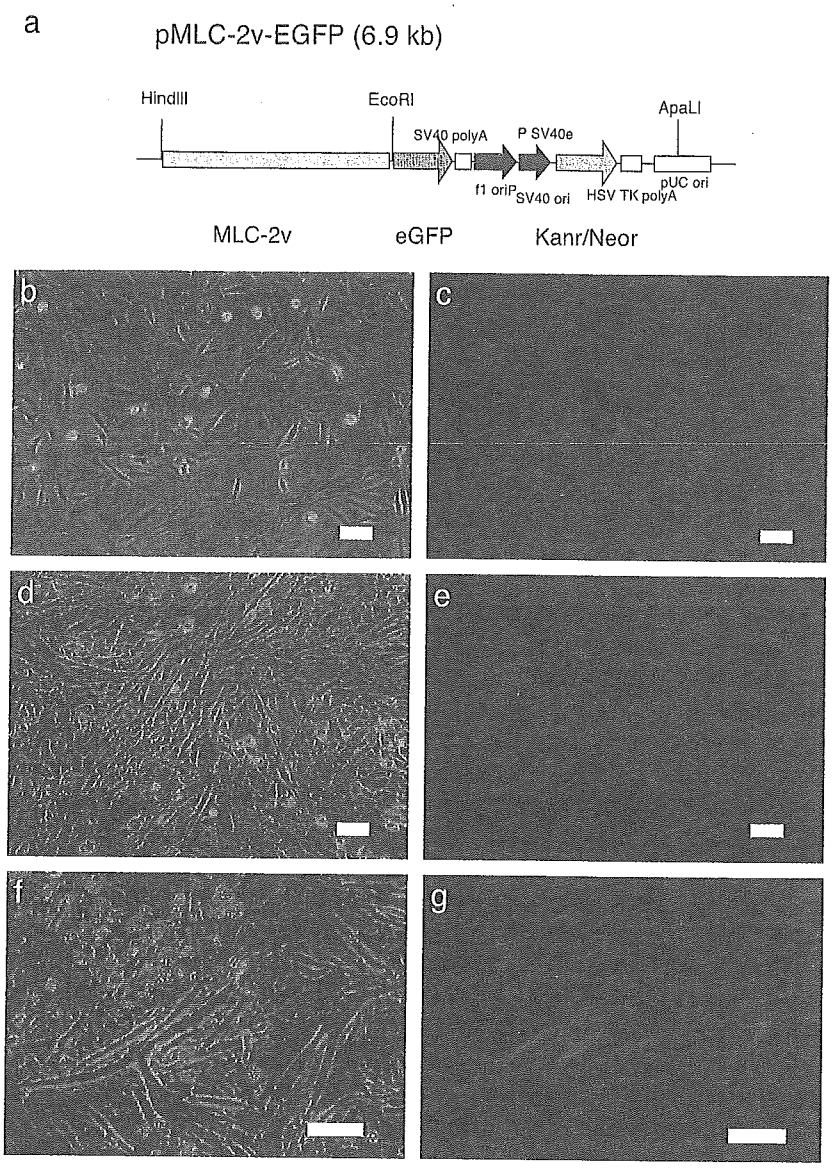

Fig. 1. Construction of pMLC-2v-EGFP and expression of EGFP in differentiated CMG cells. (a) Restriction map of pMLC-2v-EGFP. (b–g) Microscopy of the pMLC-2v-EGFP stably transfected CMG cells. b, d, and f shows phase contrast microscopy of the CMG cells after differentiation, and c, e, and g represent fluorescent microscopic views of the same field in b, d, and f. (b, c) 3 days, (d, e) 7 days, and (f, g) 4 weeks after the 5-azacytidine exposure. Bars indicate 100 μm.

with PBS containing Adex-LacZ virus at 10 MOI for 100 min. The cells were washed three times to remove virus remaining on the cell surface. Prior to transplantation, the cells were incubated in IMDM with 20% FBS for 2 days.

2.6. Transmission electron microscopy

Cells were washed three times with PBS (pH 7.4) prior to transmission electron microscopy. Cells were initially fixed with PBS containing 2.5% glutaraldehyde for 2 h. The cells were then embedded in epoxy resin. Ultra-thin sections cut horizontally to the growing surface were double stained in uranyl acetate and lead citrate, and viewed under a JEM-1200EX transmission electron microscope.

2.7. Bromodeoxyuridine (BrdU) incorporation

To detect nuclei undergoing DNA synthesis, cells were incubated with BrdU (10 μM) for 5 h, rinsed with PBS, and then fixed in methanol for 20 min at 4 °C. Immunofluorescence microscopy using a monoclonal antibody against BrdU was performed as described previously [14]. The percentage of BrdU-positive cells was estimated by counting cells on photographs of randomly chosen fields.

2.8. Gene expression analysis

Total RNA was extracted from EGFP(+) cells isolated at 7 days following transfection. RT-PCR was performed to detect α-myosin heavy chain (MHC), β-MHC, α-

skeletal actin, α-cardiac actin, myosin light chain-2v (MLC-2v), MLC-2a, Cav1.2, myoD, calponin, and α-smooth muscle actin genes. The primers and PCR cycles used were as described previously [6,15,16]. Primers for Cav1.2 were CTGCAGGTGATGATGAGGTC for the forward primer and GCGGTGTTGTTGGCGTTGTT for the reverse primer.

2.9. Immunostaining

Cells were attached to gelatin-coated glass slides, fixed in 4% paraformaldehyde, and then stained with primary antibodies against anti-GATA4, anti-troponin I, and anti-MEF2C antibodies (all from Santa Cruz Biotechnology), or anti-connexin43 antibody (Sigma). Anti-goat-IgG conjugated with Texas red or anti-rabbit IgG conjugated with Rhodamine (1:500, Pharmingen) was use as a secondary antibody.

2.10. Action potential recording

Electrophysiological studies were performed in IMDM containing (mmol/L) $CaCl_2$ 1.49, KCl 4.23, and HEPES 25 (pH 7.4). Cultured cells were placed on the stage of an inverted phase contrast optic (Diaphoto-300, Nikon) at 23 °C. Action potentials were recorded using conventional microelectrodes as described previously [8]. Intracellular recordings were taken from MLC2v-EGFP-purified cells 3 weeks following transfection.

2.11. Cell transplantation

Animal Care and Use Committees of Keio University approved all experimental procedures and protocols. Female scid mice (12 weeks) were anesthetized initially with ether and placed on a warm pad maintained at 37 °C. The trachea was cannulated with a polyethylene tube connected to a respirator (Shinano, Tokyo, Japan) with a tidal volume set at 0.6 ml and a rate set at 110/min. Mice were then anesthetized with 0.5–1.5% isoflurene under controlled ventilation with a respirator for the remainder of the surgical procedure. A left thoracotomy was performed between ribs 4 and 5, and the pericardial sac was removed. Isolated EGFP(+) cells that had been expanded for 5 days were resuspended in PBS at a concentration of 5×10^7 cells/ml. A total cell suspension volume of 50 μl was drawn into a 50 μl Hamilton syringe with a 31-gauge needle, and 10 μl was injected into the anterior wall of the left ventricle. Following the transplantation, residual cells in the syringe were collected and stained with trypan blue. The total and living cell numbers were counted. The number of living cells to inject was calculated by the following formula. (The injected living cells)=[(Total injected cells)−(Residual cells in the syringe)](Percent of living cells). Injection of PBS was used as a control.

2.12. Histological studies

The mice were sacrificed, and the hearts were dissected and fixed in 2% formaldehyde and 0.2% glutaraldehyde in PBS at room temperature for 5 min. The hearts were then washed in PBS and then incubated overnight in X-gal solution (1 mg/ml X-gal, 15 mmol/L potassium ferricyanide, 15 mmol/L potassium ferrocyanide, and 2 mmol/L $MgCl_2$ in PBS). The hearts were refixed in the same fix solution, embedded in paraffin, and sectioned into 6-μm-thick slices for hematoxylin–eosin staining. The numbers of X-gal-stained CMG cells were counted using serial sections of the transplanted heart (more than 200 slices/mouse), and an estimate of total transplanted cell survival was obtained using the following formula. (Percent of cells surviving in the recipient heart)=[(Total surviving cells in the recipient heart)/(Injected living cells)]100.

To observe EGFP fluorescence, the hearts were embedded in OCT compound and frozen with liquid nitrogen. A cryostat was used to generate 6-μm-thick sections. The samples were examined with a confocal LASER microscope (LSM510; Carl Zeiss, Jena, Germany). The GFP signal was confirmed by emission finger printing, using the LSM 510 Meta spectrometer (Carl Zeiss).

2.13. Electrocardiography (ECG) recording

ECG recordings were performed 2 and 4 weeks after transplantation. Mice were anesthetized with ether, needle limb leads were fixed, and the ECG was recorded for 1 h.

2.14. Statistics

Values are presented as mean±SD. The significance of differences among mean values was determined by ANOVA. Statistical comparison of the control and treated groups was carried out using the nonparametric Fisher's multiple comparison tests. The level accepted for significance was $p<0.05$.

3. Results

3.1. Regenerated cardiomyocytes, but not other cell types, express EGFP

G418-resistant cells were exposed to 5-azacytidine and after 3 days EGFP(+) cells exhibited a fibroblast-like morphology (Fig. 1b,c), and were difficult to distinguish from other cell types. After 7 days, the EGFP(+) cells displayed a spindle-like morphology (Fig. 1d,e), but did not spontaneously beat at this stage. After 3 weeks, the EGFP(+) cells began to appear more rod-like and form inter-cell connections and after 4 weeks spontaneous beating was observed (Fig. 1f,g). Some fractions of the EGFP(−)

cells differentiated into adipocytes, but other EGFP(−) cells did not display any specific morphology. These findings indicate that the MLC2v–EGFP system may be a useful method for distinguishing regenerated cardiomyocytes from other cell types at an early stage.

3.2. Fluorescence-activated cell sorting (FACS) analysis

FACS analysis was performed 3 day after 5-azacytidine exposure to isolate regenerated cardiomyocytes. Control cells (before 5-azacytidine exposure) showed no detectable fluorescence (Fig. 2a), whereas 3 days after 5-azacytidine exposure the cells stable transfected with the MLC2v-EGFP expression plasmid generated sufficient EGFP signal for cell sorting (Fig. 2b). The EGFP(+) fraction ranged from 6–24%. Fig. 2c,d shows the cells 4 days after cell sorting (7 days after 5-azacytidine exposure) displaying a fibroblast-like morphology. The percentage of EGFP-positive cells was calculated by comparing cell counts from phase contrast microscopy with EGFP(+) cell counts using fluorescence microscopy, 3 days after cell sorting. More than 99% of the sorted cells expressed EGFP fluorescence. After 3 weeks, these cells had a spindle-like appearance and began spontaneous beating (Fig. 2e,f).

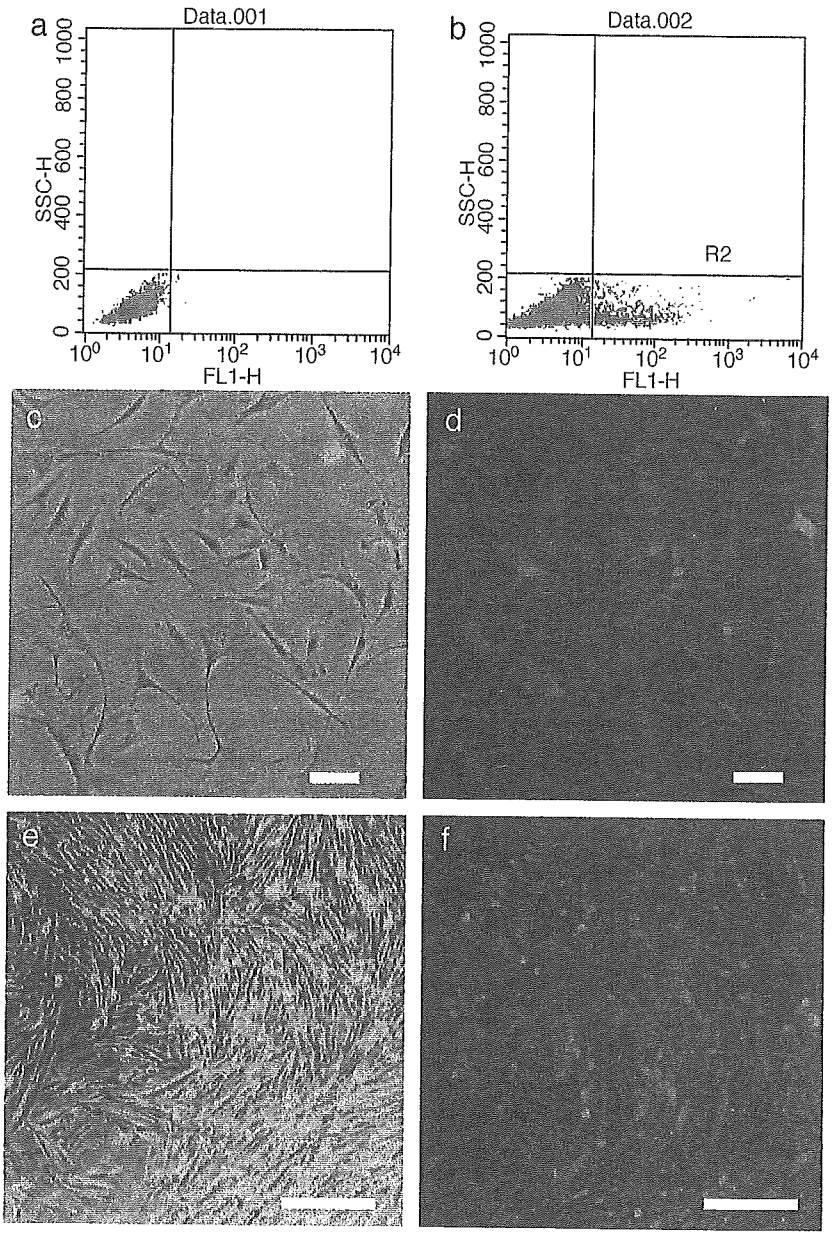

Fig. 2. FACS analysis of the pMLC-2v-EGFP-transfected cells and microscopy of the sorted cells. (a, b) FACS analysis of the pMLC-2v-EGFP-transfected cells. The horizontal axis indicates the intensity of EGFP fluorescence. (a) Control cells, (b) cells 3 days after exposure to 5-azacytidine exposure. d and f are fluorescence microscopy images of the EGFP signal. c and e are phase contrast microscopy views of the same field. (c, d) 4 days, and (e, f) 3 weeks after cell sorting. Note that all the cells display EGFP fluorescence, and that the EGFP(+) CMG cells exhibit a cardiomyocyte-like appearance and spontaneously beat after 3 weeks. Bars in c,d and e,f indicate 100 and 500 μm, respectively.

3.3. Character of the sorted EGFP(+) regenerated cardiomyocytes

A total of 768 single EGFP(+) cell clones were isolated using FACS analysis. Although EGFP(+) cells undergo cell division after 5-azacytidine exposure, a cardiomyocyte cell line could not be generated as cells stop proliferating after several cell divisions. The cells were exposed to BrdU to confirm their mitogenicity, and double immunostaining was performed with antisarcomeric myosin and anti-BrdU antibodies. Myosin-positive cells incorporated BrdU until day 5, but stopped incorporating it after day 7 (Fig. 3a). This finding shows that the mitogenicity of the isolated EGFP(+) CMG cells is limited, so it can be assumed that the risk of cardiomyosarcoma formation is negligible.

RT-PCR analysis of cardiac contractile proteins revealed that the isolated EGFP(+) CMG predominantly express the β-myosin heavy chain, α-skeletal-actin, and MLC-2v, indicating that the phenotype of these cells represents fetal ventricular cardiomyocytes. These cells also express cardiac L-type Ca^{2+} channels but did not express myogenic genes such as myoD, or smooth-muscle-specific genes, such as calponin or α-smooth muscle actin genes (Fig. 3b).

3.4. Action potential recording

MLC2v-EGFP-selected cells showed regular spontaneous beating 3 weeks following selection. The action potentials of these cells had a relatively shallow resting membrane potential with a late diastolic slow depolarization, like a pacemaker potential. They also displayed peak-notch-plateau characteristics representative of ventricular cardiomyocyte-like action potentials (Fig. 3c).

3.5. Immunostaining and transmission electron microscopy

Immunostaining revealed that EGFP(+) but not EGFP(−) CMG cells express cardiac troponin I (Fig. 4a–d). EGFP(+) CMG cells express both GATA4 and MEF2C, respectively (Fig. 4e,f). Interestingly, EGFP(−) CMG cells express GATA4 and Nkx2.5. These findings are consistent with the previous report that these cardiac transcription factors are expressed before final 5-azacytidine exposure [6]. EGFP(+) CMG cells also express connexin43 (Fig. 4g).

The sorted GFP(+) cells were cultured for 2 weeks, fixed, and processed for transmission electron microscopy. The typical contractile apparatus of the sarcomeres, including striation pattern, was observed (Fig. 4h).

3.6. Cell transplantation study

Animals with transplanted EGFP(+) cells were sacrificed at 2, 4, 8, and 12 weeks. Confocal LASER microscopy revealed that the EGFP(+) transplanted cardiomyocytes survived in the recipient heart (Fig. 5a–c). The control experiment revealed no EGFP(+) transplanted cardiomyocytes (data not shown) [17]. The orientation of the transplanted cells was consistent with the cardiomyocytes of the recipient heart. The EGFP(+) cells were observed only at the site of injection in the left ventricle and in no other parts of the heart. We also confirmed that these green signals were

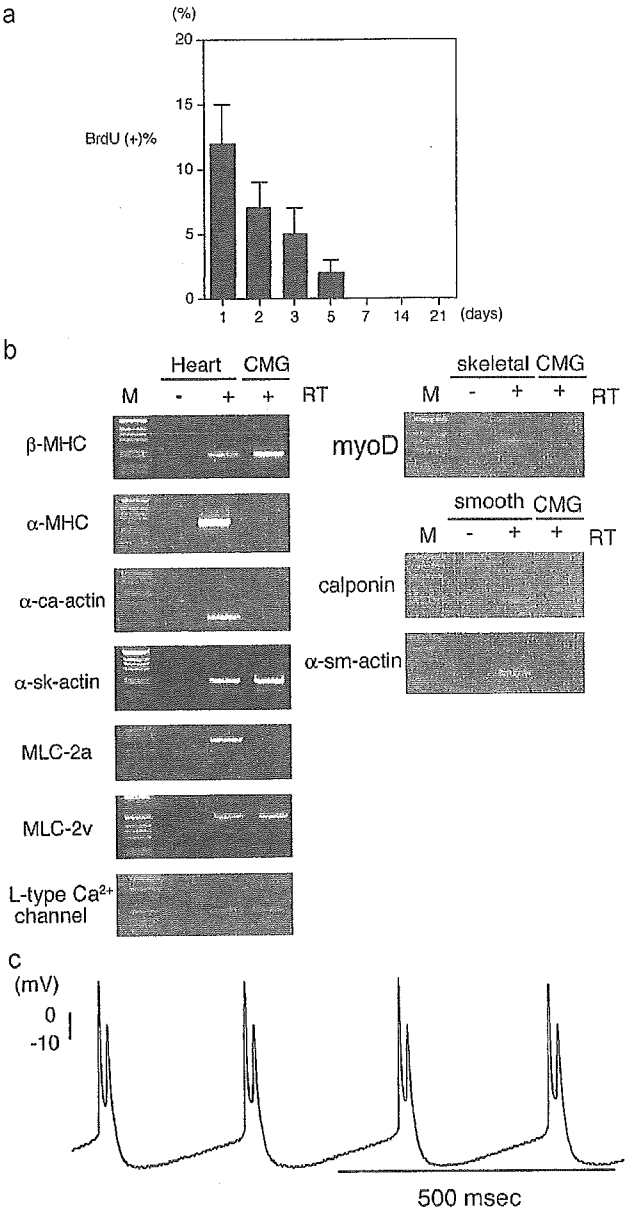

Fig. 3. Characteristics of the sorted CMG cardiomyocytes. (a) BrdU incorporation of EGFP(+) CMG cells after cell sorting. BrdU was loaded for 5 h, and its incorporation was detected. BrdU incorporation was observed until 5 days after cell sorting (8 days after 5-azacytidine exposure). (b) Phenotype of the EGFP(+) CMG cells. RT-PCR was performed for α-MHC, β-MHC, MLC-2v, MLC-2a, α-skeletal actin, α-cardiac actin, and cardiac α1c Ca^{2+} channel. The expression pattern of the cardiac contractile protein indicated that these cells had the fetal ventricular phenotype. MLC-2v-EGFP selected cells did not express myoD, calponin, and α-smooth muscle actin genes. Femoral muscle, which includes vascular smooth muscle cells, were used as a positive control. M: 1-kb DNA ladder. RT: reverse transcription. (c) The representative tracing of the action potentials at 3 weeks after cell sorting was shown. These action potentials show ventricular cardiomyocyte-like action potentials.

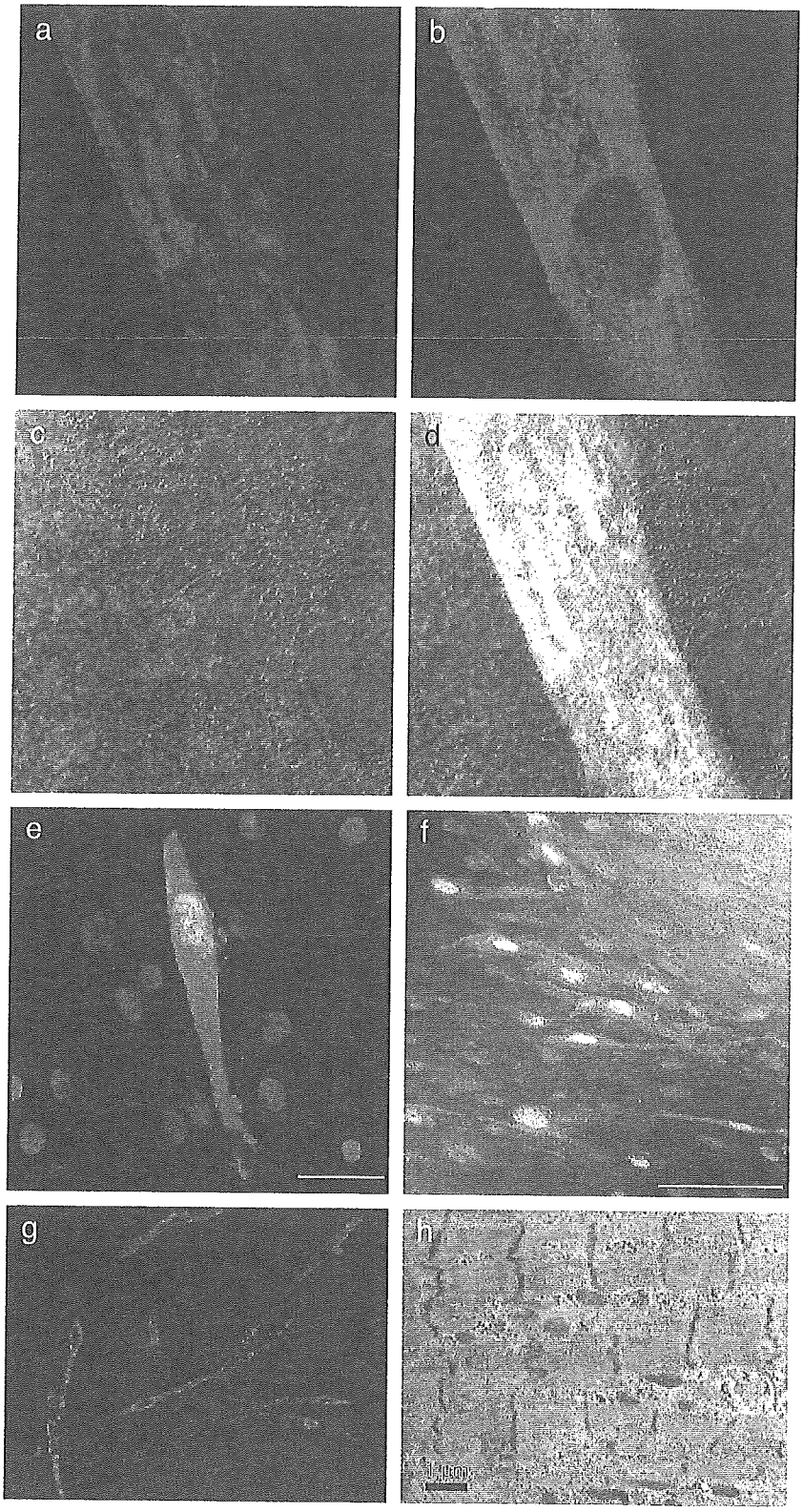

Fig. 4. Photograph of immunofluorescence and transmission electron micrograph of CMG cells. (a–d) EGFP(+) and EGFP(−) CMG cells were stained with anti-troponin I antibodies (a) and DAPI (c). EGFP(+) CMG cells expressed troponin I, but EGFP(−) CMG cell did not express troponin I. (e) Immunofluorescent staining with GATA4. Both EGFP(+) and EGFP(−) CMG cells expressed GATA4. (f) Immunofluorescent staining with MEF2C. Both EGFP(+) and EGFP(−) CMG cells expressed MEF2C. (g) Immunofluorescent staining with connexin43. EGFP(+) CMG cells expressed connexin43. (h) Transmission electron microscopy of the CMG cells showed typical contractile apparatus.

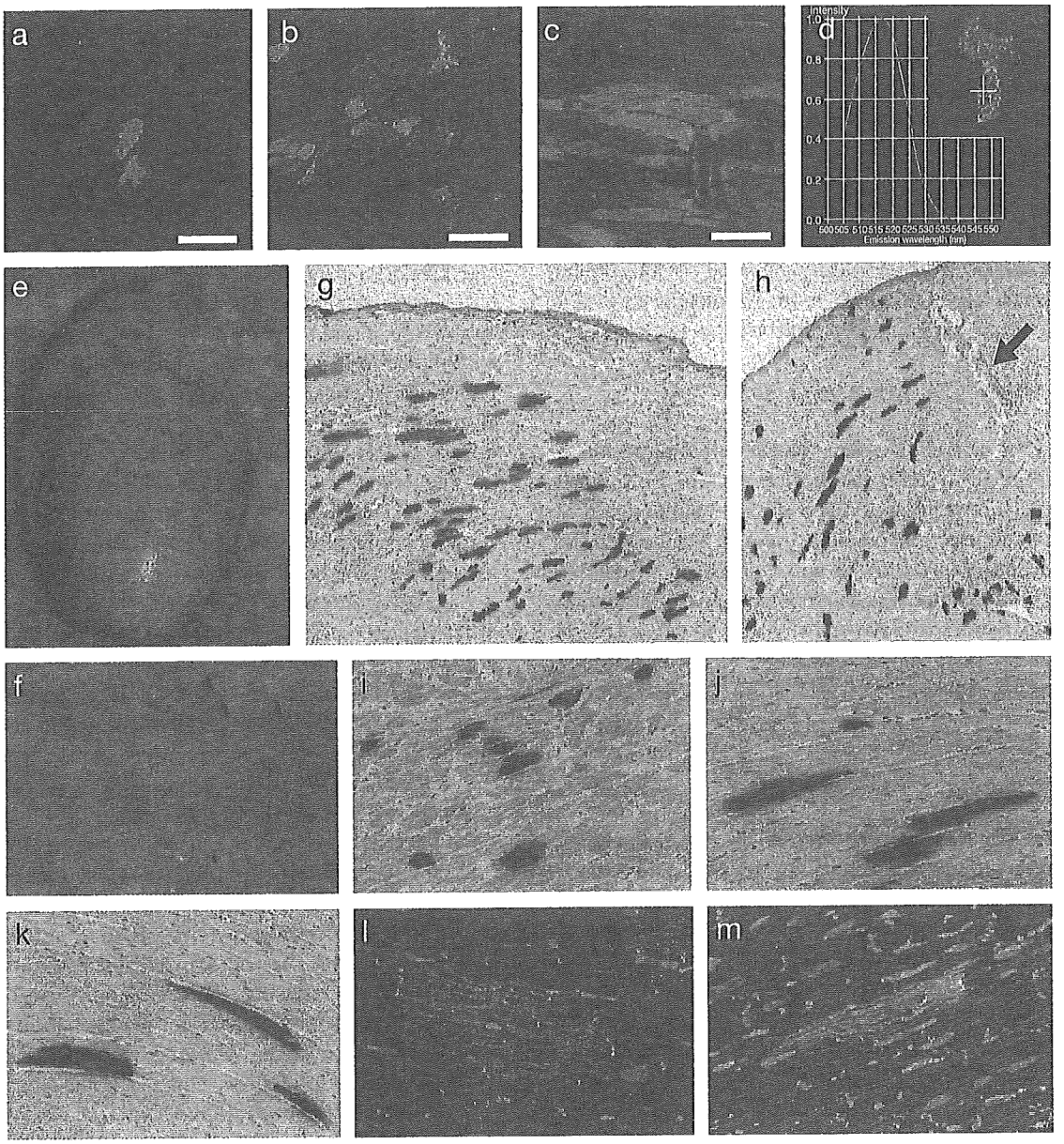

Fig. 5. Histological analysis of the transplanted CMG cells. (a–c) Confocal microscopy of the recipient heart transplanted with the sorted cardiomyocytes at 4 weeks. The transplanted cells could be clearly identified by EGFP signals. a and b show the transverse section of the transplanted cardiomyocytes, and c shows the longitudinal section. Bars indicate 50 μm. (d) The emission profile of the green signal in GFP^+ cells was investigated by CLSM. The emission peak existed at 510–530 nm, and the profile was ascertained to be that of GFP, and not arising from nonspecific background. The inset shows the GFP^+ transplanted cells, and the cross indicates the site of the emission profile. (e–m) The bone-marrow-derived cardiomyocytes were sorted and marked with adenovirus-mediated LacZ gene. e is a photograph of the whole heart, and f shows an enlarged photograph of the injected site. The transplanted LacZ-positive cells were identified from the surface. g and h show the microscopy of the injected site of the left ventricle. The samples were stained with LacZ and hematoxylin–eosin. i–k show higher magnification of the same fields: i shows the transverse section, and j,k show the longitudinal section. (l, m) Transplanted CMG cells were stained with anticonnexin43 antibody and DAPI. Connexin43 was expressed at the both ends of the transplanted EGFP(+) CMG cells. Green: EGFP, Blue: DAPI, Red: connexin43.

not due to nonspecific background fluorescence, but due to the EGFP itself, using absorbance frequency analysis on a LSM510 Meta spectrometer (Fig. 5d).

Fig. 5e shows the entire murine heart stained with LacZ at 4 weeks after transplantation, and Fig. 5f showed an enlarged photograph of the site of injection. Cells were transplanted into the anterior free wall of the left ventricle and were observed to be rectangular in shape and located at the surface of the heart. Fig. 5g,h shows the site of injection in a transverse section of the left ventricle stained with LacZ and hematoxylin–eosin 4 weeks after transplantation. The scar of the injection needle is shown in Fig. 5h. Granulomatous tissue was also observed around the site of injection. The LacZ-stained transplanted cells were clearly visible, and were located throughout the site of injection. Fig. 5i–k shows transverse and longitudinal sections of the transplanted cardiomyocytes at higher magnifications. This figure clearly shows the arrangement of the transplanted

cells parallel to the cardiomyocytes of the recipient heart. Fig. 5l,m shows expression of connexin43 at the longitudinal border between transplanted EGFP(+) CMG cells and adjacent cardiomyocytes of the recipient heart.

Transplanted cardiomyocytes survived in the recipient heart for more than 3 months and the estimated percentage of cells surviving transplantation was 6.5±3.2%. Table 1 shows the diameter of transplanted cardiomyocytes in transverse section. The diameter increased to almost the same size as the cardiomyocytes in the recipient heart over 4 weeks after which time no further increase was observed.

3.7. ECG recording and survival curve

Of the 35 mice that had undergone cell transplantation, 5 died within 24 h. This is most likely a result of the surgical procedure. The remaining 30 mice survived the duration of the observation period. ECGs recordings in 5 mice at 2 and 4 weeks, respectively, showed no evidence of arrhythmia (ventricular premature beats, ventricular tachycardia) during the recording period (data not shown). This finding suggests that survival of recipients in this model is not affected by arrhythmia.

4. Discussion

Since our report that cardiomyocytes can be regenerated from bone marrow stem cells [6,7], several studies have shown that transplantation of bone-marrow mononuclear cells or bone marrow stem cell fractions into the heart can improve cardiac function. Although the direct transplantation of these cells omits prior differentiation or purification, and thereby shortens the therapeutic period, it remains undetermined whether transplanted cells differentiate into the desired cardiomyocytes or endothelial cells, and not into other cell types including osteoblasts, chondroblasts, or adipocytes. The establishment of a reliable method to repair injured myocardium using cardiomyocyte transplantation requires the preparation of a sufficient number of well-characterized, purified regenerated cardiomyocytes, and an estimation of the survival rate of the transplanted cells.

Tomita [18] reported that the transplantation of 5-azacytidine-treated primary cultured marrow-stromal cells improved the function of the infarcted myocardium. Since the population of mesenchymal stem cells in primary cultured mice marrow stromal cells is less than 0.01%, it is likely that most of the cells transplanted do not differentiate into cardiomyocytes, and that the observed improvement in cardiac function is caused by an improvement in ventricular remodeling or stimulation of angiogenesis.

Jackson transplanted adult stem cells [CD34(−)/low, c-Kit(+), Sca-1(+)] into lethally irradiated mice subsequently rendered ischemic by coronary artery occlusion followed by reperfusion, and reported that the engrafted cells migrated into ischemic cardiac muscle and blood vessels, differentiated to cardiomyocytes and endothelial cells, and contributed to the formation of functional tissue [19]. They found that the donor-derived endothelial cells were present at around 3.3%, primarily in small vessels adjacent to the infarct, and that donor-derived cardiomyocytes were present at around 0.02% and were found primarily in the peri-infarct region. Taken together, these findings show that differentiation from marrow stromal cells to cardiomyocytes in vivo is possible, but that their prevalence is less than other cell types. Condrelli [20] reported that neural stem cells differentiated into heart muscle cells when mixed with heart muscle cells from newborn rats in a process known as transdifferentiation. The mechanism of in vitro transdifferentiation is based on the idea that the developmental limitations of tissue specific stem cells are dictated by the environment, and that new signals that relax these limitations may be provided by cells from a different tissue [20].

It is most likely that the direct transplantation of stem cells into the heart does not facilitate their differentiation into cardiomyocytes, but merely results in their fusion with residual cardiomyocytes. We propose a more rigorous method to achieve repair of damaged tissue by first differentiation adult stem cells cardiomyocytes in vitro, and then transplanting a sufficient number of differentiated cardiomyocytes into the damaged heart tissue. To avoid possible adverse effects, we emphasize the importance of thoroughly investigating the molecular and electrophysiological characteristics of the stem cell-derived regenerated cardiomyocytes prior to transplantation.

In the present study, we used an EGFP reporter gene under the control of the MLC-2v promoter to tag isolated cardiomyocytes. Following FACS analysis, 99% of the isolated cardiomyocytes expressed EGFP, and when transplanted into the recipient heart they survived for at least 4 weeks. We observed no other cell types in the transplanted area, but this may have been because we only used a strongly expressing EGFP(+) fraction.

Table 1
Diameter of the transplanted bone-marrow-derived cardiomyocyte

Time after transplantation (weeks)	2	4	8	12	Recipient cardiomyocytes
Diameter (μm)	10.5±3.6*	19.0±4.8$	19.1±5.0$	19.1±4.9$	19.5±5.1

The diameter of the transplanted cardiomyocytes was measured by the transverse section of the recipient hearts. Each data was obtained by measuring 200 cells. Mean±SD. $: not significant vs. recipient cardiomyocytes.

* $p<0.01$ vs. 4 weeks and recipient cardiomyocytes.

A plasmid encoding reporter genes and cardiac specific gene promoters was used in a previous study to isolate cardiomyocytes from ES cells or embryonic carcinoma cells (EC cell) [21]. Klug et al. [8] transfected a fusion gene containing the α-myosin heavy chain (α-MHC) promoter and aminoglycoside phosphotransferase (NeoR) into pluripotent ES cells, then differentiated these cells in vitro prior to G418 selection. They reported high purification (>99%) and a survival period in the recipient heart of at least 7 weeks following transplantation. Zweigerdt et al. [22] and Zandstra et al. [23] reported a lab-scale protocol to generate cultures of highly enrich cardiomyocyte from ES cells transfected with a α-MHC-NeoR containing plasmid, and suggest its application to a larger-scale process for the supply of stem cell based cardiomyocytes. Muller et al. [9] isolated a subpopulation of ventricular-like cardiomyocytes from ES cells by transfecting the EGFP gene under the control of the MLC-2v promoter and cytomegalovirus enhancer. Moore et al. [24] reported that EC cell (P19Cl6)-derived cardiomyocytes could be isolated using an EGFP reporter under the control of 250 bp of the MLC-2v promoter. They enzymatically digested embryoid bodies, then isolated a population of cardiomyocytes (97% pure) using Percoll gradient centrifugation and FACS analysis. Kolossov et al. [25] reported the use of EGFP under the control of the cardiac α-actin promoter to isolate ES cell-derived cardiomyocytes. The present study confirmed the efficiency of this strategy for the isolation and purification of cardiomyocytes from bone-marrow-derived stem cells.

Reinecke and Murry [26] and Zhang et al. [27] highlighted the importance of a quantitative analysis of grafted cardiomyocytes, since a large number of fetal or neonatal cardiomyocytes often display apoptosis within several days of transplantation. They reported that only a small percentage of cardiomyocytes survive in the cryoinjured recipient heart, and that heat shock or adenoviral transfer of constitutive active Akt genes could increase their survival. In comparison, the present study reports a slightly higher survival rate for bone marrow-derived cardiomyocytes. One possible reason is the difference in the experimental models as the present study used a mouse uninjured model and not a rat cryoinjured heart model. Another reason is the small size of our not fully differentiated transplanted cells compared with fetal or neonatal cardiomyocytes. A small size may allow transplanted cells to go deep into the recipient heart without mechanical injury.

Recently, Takeda et al. [28] reported that the life span of human bone marrow mesenchymal stem cells could be prolonged by infecting the cells with the retrovirus encoding oncogene bmi-1, human papilloma virus E6 and E7, and human telomerase reverse transcriptase over 150 population doublings, and that these cells could be induced to differentiate into cardiomyocyte using 5-azacytidine and co-culture with the rat cardiomyocytes. Although this procedure is not suitable for clinical application at the present stage, the findings provide valuable information on the use of human bone marrow stem cells for the regeneration of cardiomyocytes.

In summary, the present study provides a new model for tissue engineering. Further studies are required to improve cardiomyocyte differentiation and to increase the efficiency of the transplantation procedure.

Acknowledgements

This study was supported in part by the research grants (10B-1) of "Nervous and Mental Disorders from the Ministry of Health and Welfare", Japan, the research grants from the Ministry of Education, Science and Culture, Japan, and the research grants from Health Science Research Grants for Advanced Medical Technology from the Ministry of Welfare, Japan.

References

[1] Leor J, Patterson M, Quinones MJ, Kedes LH, Kloner RA. Transplantation of fetal myocardial tissue into the infarcted myocardium of rat A potential method for repair of infarcted myocardium? Circulation 1996;94(Suppl. 9):II332–6.
[2] Matsushita T, Oyamada M, Kurata H, Masuda S, Takahashi A, Emmoto T, et al. Formation of cell junctions between grafted and host cardiomyocytes at the border zone of rat myocardial infarction. Circulation 1999;100(Suppl. 19):II262–8.
[3] Sakai T, Li RK, Weisel RD, Mickle DA, Kim EJ, Tomita S, et al. Autologous heart cell transplantation improves cardiac function after myocardial injury. Ann Thorac Surg 1999;68:2074–80.
[4] Weissman IL. Translating stem and progenitor cell biology to the clinic: barriers and opportunities. Science 2000;287:1442–6.
[5] Weissman IL, Anderson DJ, Gage F. Stem and progenitor cells: origins, phenotypes, lineage commitments, and transdifferentiations. Annu Rev Cell Dev Biol 2001;17:387–403.
[6] Makino S, Fukuda K, Miyoshi S, Konishi F, Kodama H, Pan J, et al. Cardiomyocytes can be generated from marrow stromal cells in vitro. J Clin Invest 1999;03:697–705.
[7] Hakuno D, Fukuda K, Makino S, Konishi F, Tomita Y, Manabe T, et al. Bone marrow-derived cardiomyocytes (CMG cell) expressed functionally active adrenergic and muscarinic receptors. Circulation 2002;105:380–6.
[8] Klug MG, Soonpaa MH, Koh GY, Field LJ. Genetically selected cardiomyocytes from differentiating embryonic stem cells form stable intracardiac grafts. J Clin Invest 1996;98:216–24.
[9] Muller M, Fleischmann BK, Selbert S, Ji GJ, Endl E, Middeler G, et al. Selection of ventricular-like cardiomyocytes from ES cells in vitro. FASEB J 2000;14:2540–8.
[10] O'Brien TX, Lee KJ, Chien KR. Positional specification of ventricular myosin light chain 2 expression in the primitive murine heart tube. Proc Natl Acad Sci U S A 1993;90:5157–61.
[11] Henderson SA, Spencer M, Sen A, Kumar C, Siddiqui MA, Chien KR. Structure, organization, and expression of the rat cardiac myosin light chain-2 gene. Identification of a 250-base pair fragment which confers cardiac-specific expression. J Biol Chem 1989;264:18142–8.
[12] Kanegae Y, Makimura M, Saito I. A simple and efficient method for purification of infectious recombinant adenovirus. Jpn J Med Sci Biol 1995;47:157–66.
[13] Niwa H, Yamamura K, Miyazaki J. Efficient selection for high-expression transfectants by a novel eukaryotic vector. Gene 1991;108:193–200.

[14] Fukuda K, Izumo S. Angiotensin II potentiates DNA synthesis in AT-1 transformed cardiomyocytes. J Mol Cell Cardiol 1998;30: 2069–80.
[15] Myer A, Olson EN, Klein WH. MyoD cannot compensate for the absence of myogenin during skeletal muscle differentiation in murine embryonic stem cells. Dev Biol 2001;229:340–50.
[16] Yamada H, Akishita M, Ito M, Tamura K, Daviet L, Lehtonen JY, et al. AT2 receptor and vascular smooth muscle cell differentiation in vascular development. Hypertension 1999;33:1414–9.
[17] Jackson KA, Snyder DS, Goodell MA. Skeletal muscle fiber-specific green autofluorescence: potential for stem cell engraftment artifacts. Stem Cells 2004;22:180–7.
[18] Tomita S, Li RK, Weisel RD, Mickle DA, Kim EJ, Sakai T, et al. Autologous transplantation of bone marrow cells improves damaged heart function. Circulation 1999;100(Suppl. 19):II247.
[19] Jackson KA, Majka SM, Wang H, Pocius J, Hartley CJ, Majesky MW, et al. Regeneration of ischemic cardiac muscle and vascular endothelium by adult stem cells. J Clin Invest 2001;107:1395–402.
[20] Condorelli G, Borello U, De Angelis L, Latronico M, Sirabella D, Coletta M, et al. Cardiomyocytes induce endothelial cells to trans-differentiate into cardiac muscle: Implications for myocardium regeneration. Proc Natl Acad Sci U S A 2001;98:10733–8.
[21] Sachinidis A, Fleischmann BK, Kolossov E, Wartenberg M, Sauer H, Hescheler J. Cardiac specific differentiation of mouse embryonic stem cells. Cardiovasc Res 2003;58:278–91.
[22] Zweigerdt R, Burg M, Willbold E, Abts H, Ruediger M. Generation of confluent cardiomyocyte monolayers derived from embryonic stem cells in suspension: a cell source for new therapies and screening strategies. Cytotherapy 2003;5:399–413.
[23] Zandstra PW, Bauwens C, Yin T, Liu Q, Schiller H, Zweigerdt R, et al. Scalable production of embryonic stem cell-derived cardiomyocytes. Tissue Eng 2003;9:767–78.
[24] Moore JC, Spijker R, Martens AC, de Boer T, Rook MB, van der Heyden MA, et al. A P19Cl6 EGFP reporter line to quantify cardiomyocyte differentiation of stem cells. Int J Dev Biol 2004;48:47–55.
[25] Kolossov E, Fleischmann BK, Liu Q, Bloch W, Viatchenko-Karpinski S, Manzke O, et al. Functional characteristics of ES cell-derived cardiac precursor cells identified by tissue-specific expression of the green fluorescent protein. J Cell Biol 1998;143:2045–56.
[26] Reinecke H, Murry CE. Taking the death toll after cardiomyocyte grafting: a reminder of the importance of quantitative biology. J Mol Cell Cardiol 2002;34:251–3.
[27] Zhang M, Methot D, Poppa V, Fujio Y, Walsh K, Murry CE. Cardiomyocyte grafting for cardiac repair: graft cell death and anti-death strategies. J Mol Cell Cardiol 2001;33:907–21.
[28] Takeda Y, Mori T, Imabayashi H, Kiyono T, Gojo S, Miyoshi S, et al. Can the life span of human marrow stromal cells be prolonged by bmi-1, E6, E7, and/or telomerase without affecting cardiomyogenic differentiation? J Gene Med 2004;6:833–45.

Journal of the American College of Cardiology
© 2005 by the American College of Cardiology Foundation
Published by Elsevier Inc.

Vol. 45, No. 4, 2005
ISSN 0735-1097/05/$30.00
doi:10.1016/j.jacc.2004.10.053

PRECLINICAL RESEARCH

Beneficial Effect of Hydroxyfasudil, a Specific Rho-Kinase Inhibitor, on Ischemia/Reperfusion Injury in Canine Coronary Microcirculation In Vivo

Toyotaka Yada, MD, PHD,* Hiroaki Shimokawa, MD, PHD,† Osamu Hiramatsu, PHD,* Tatsuya Kajita, MD, PHD,* Fumiyuki Shigeto, MD, PHD,* Etsuro Tanaka, MD, PHD,‡ Yoshiro Shinozaki, BS,§ Hidezo Mori, MD, PHD,‖ Takahiko Kiyooka, MD,# Masashi Katsura, PHD,¶ Seitaro Ohkuma, MD, PHD,¶ Masami Goto, MD, PHD,* Yasuo Ogasawara, PHD,* Fumihiko Kajiya, MD, PHD#

Kurashiki, Fukuoka, Tokyo, Isehara, Suita, and Okayama, Japan

OBJECTIVES We examined whether hydroxyfasudil, a specific Rho-kinase inhibitor, exerts cardioprotective effect on coronary ischemia/reperfusion (I/R) injury and, if so, whether nitric oxide (NO) is involved.

BACKGROUND Recent studies have demonstrated that Rho-kinase is substantially involved in the pathogenesis of cardiovascular diseases; however, it remains to be examined whether it is also involved in ischemia/reperfusion (I/R) injury.

METHODS Canine subepicardial small arteries (SA, ≥100 μm) and arterioles (A, <100 μm) were observed by a charge-coupled device intravital microscope during I/R. Coronary vascular responses to endothelium-dependent (acetylcholine, intracoronary [IC]) and -independent (papaverine, IC) vasodilators were examined after I/R under the following four conditions: control (n = 7), NO synthase inhibitor alone (N^G-monomethl-L-arginine [L-NMMA], IC, n = 4), hydroxyfasudil alone (IC, n = 7), and hydroxyfasudil plus L-NMMA (n = 7).

RESULTS Hydroxyfasudil significantly attenuated serotonin (IC)-induced vasoconstriction of SA (−7 ± 1% vs. 2 ± 1%, $p < 0.01$). Coronary I/R significantly impaired coronary vasodilation to acetylcholine after I/R (SA, $p < 0.05$; and A, $p < 0.01$ vs. before I/R) and L-NMMA further reduced the vasodilation, whereas hydroxyfasudil completely preserved the responses. The vasoconstriction by L-NMMA after I/R was significantly improved by hydroxyfasudil in both-sized arteries (both $p < 0.01$). Expression of endothelial nitric oxide synthase (eNOS) protein in the ischemic endocardium of left anterior descending coronary artery area (as determined by Western blotting) significantly decreased (79 ± 4%) compared with the nonischemic endocardium of LCX area (100 ± 7%), which was improved by hydroxyfasudil (105 ± 6%, $p < 0.01$). Hydroxyfasudil significantly reduced myocardial infarct size, and hydroxyfasudil with L-NMMA also reduced the infarct size compared with L-NMMA alone.

CONCLUSIONS Hydroxyfasudil exerts cardioprotective effects on coronary I/R injury in vivo, in which NO-mediated mechanism may be involved through preservation of eNOS expression. (J Am Coll Cardiol 2005;45:599–607) © 2005 by the American College of Cardiology Foundation

Ischemia-reperfusion (I/R) injury attenuates endothelium-dependent dilation of large coronary arteries both in vitro (1,2) and in vivo (3,4). Endothelial dysfunction causes adverse outcome in the coronary circulation (5). Reperfusion injury is caused by direct myocardial injury through coronary vasospasm, free radicals, and inflammatory responses (6,7). Furthermore, local coronary vasoconstrictions in response to vasoconstrictors (e.g., serotonin) are enhanced (8,9). However, the mechanism of I/R-induced vascular injury remains to be clarified.

Recent studies have demonstrated that Rho-kinase, an effector of the small guanosine triphosphatase Rho, is substantially involved in the pathogenesis of cardiovascular diseases (10). Shimokawa et al. (10,11) have recently found that hydroxyfasudil is a potent and specific inhibitor of Rho-kinase and markedly inhibits coronary hyperconstriction and macrophage migration. They also demonstrated that intracoronary serotonin induces coronary hypercontractions at the inflammatory coronary lesions both in vitro and in vivo, in which up-regulated Rho-kinase is substantially

From the *Department of Medical Engineering and Systems Cardiology, Kawasaki Medical School, Kurashiki, Japan; †Department of Cardiovascular Medicine, Kyushu University Graduate School of Medical Sciences, Fukuoka, Japan; ‡Faculty of Applied Bioscience, Tokyo University of Agriculture, Tokyo, Japan; §Department of Physiology, Tokai University School of Medicine, Isehara, Japan; ‖Department of Cardiac Physiology, National Cardiovascular Center Research Institute, Suita, Japan; ¶Department of Pharmacology, Kawasaki Medical School, Kurashiki, Japan; and #Department of Cardiovascular Physiology, Okayama University Graduate School of Medicine and Dentistry, Okayama, Japan. This work was supported in part by grants from the Japanese Ministry of Education, Science, Sports, Culture, and Technology, Tokyo, Japan (Nos. 13307024, 13557068, 14657178, and 16300164); and the Program for Promotion of Fundamental Studies in Health Sciences of the Organization for Pharmaceutical Safety and Research of Japan.

Manuscript received September 2, 2004; revised manuscript received October 1, 2004, accepted October 18, 2004.

JACC Vol. 45, No. 4, 2005
February 15, 2005:599–607

Abbreviations and Acronyms
I/R = ischemia-reperfusion
LAD = left anterior descending coronary artery
LCX = left circumflex artery
NO = nitric oxide

involved (12). Recent studies demonstrated that endothelial expression and activity of Rho-kinase are enhanced by hypoxia, with a resultant down-regulation of endothelial nitric oxide synthase (eNOS) expression and reduced nitric oxide (NO) production (13), and that Rho-kinase is also involved in a canine model of cerebral infarction associated with superoxide production and neutrophil infiltration (14).

It is conceivable that Rho-kinase is involved in the mechanisms of I/R injury associated with reduced endothelial NO production. In this study, we thus examined whether hydroxyfasudil exerts protective effect on coronary I/R injury in vivo and, if so, whether NO is involved.

METHODS

Animal preparation. This study conformed to the Guideline on Animal Experiments of Kawasaki Medical School and the Guide for the Care and Use of Laboratory Animals published by the U.S. National Institutes of Health.

Mongrel dogs (15 to 25 kg, n = 31) of either gender were anesthetized with morphine (3 mg/kg, intramuscular) and sodium pentobarbital (25 mg/kg, intravenous). After intubation, each animal was ventilated with a high-frequency jet ventilator (model VS600, IDC, Pittsburgh, Pennsylvania) with room air supplemented by 100% oxygen. Aortic pressure and left ventricular pressure were continuously monitored with an 8-F pigtail double manometer catheter (SPC-784A, Millar, Texas). The proximal portion of the left anterior descending coronary artery (LAD) was isolated and a transonic flow probe (T206, Transonic Systems, Ithaca, New York) was placed around the vessel.

Needle-probe intravital microscope. The needle-probe (4.5 mm in diameter, VMS 1210, Nihon Kohden, Tokyo, Japan) contains a gradient index lens (with a magnification of 200) surrounded by light guide fibers and a double lumen sheath. A doughnut-shaped balloon on the tip avoids direct compression of the vessels by the needle tip (15).

Measurements of coronary diameters. We placed the needle probe gently on subepicardial microvessels. When a clear vascular image was obtained, end-diastolic vascular images were taken with 30 pictures/s (15).

Measurements of regional myocardial blood flow. Regional myocardial blood flow was determined by the nonradioactive microsphere (Sekisui Plastic Co, Ltd, Tokyo, Japan) technique, as previously described in detail (16). Briefly, 1 ml of the microspheres suspension (2 to 4 × 10^6 spheres) was injected into the left atrium 85 min after the onset of coronary occlusion. Just before microsphere administration, a reference blood flow sample was drawn from the femoral artery at a constant rate of 8 ml/min for 2 min. The X-ray fluorescence of the stable heavy elements was measured by a wavelength-dispersive spectrometer (model PW 1480, Phillips Co., Ltd., Eindhoven, the Netherlands) (16). Myocardial blood flow was calculated according to the formula: time flow = tissue counts × (reference flow/reference counts) and was expressed in ml/g per minute (16).

Western blotting. Proteins were separated on sodium dodecyl sulfate (SDS)/polyacrylamide gel electrophoresis as previously described (17). The tissues were homogenized in a sample buffer (100 mM Tris-HCl [pH 6.8], 4% SDS, 0.2% glycerol). The tissue lysate was centrifuged and the supernatant collected. Protein concentration was quantified by a bicinchoninate (BCA) protein assay kit (Pierce Chemical, Rockford, Illinois). An aliquot of 10 μg of protein from each sample was electrophoresed on a 7.5% SDS-polyacrylamide gel. Proteins were subsequently transferred to polyvinylidine difluoride membrane (Immobilon-P membrane, Millipore, Bedford, Massachusetts) electrophoretically (100 V for 1 h) and membranes were incubated with antibody. The antibodies used in this study were rabbit anti-phosphorylated ezrin/radixin/moesin (ERM) family, total ERM. The antibody against phosphorylated ERM recognizes human moesin (phosphorylated at Thr558), which also binds to the phosphorylated ezrin (Thr567) and radixin (Thr564). Therefore, we used the extent of phosphorylation of ERM as a marker of Rho-kinase activity. The levels of Western blot for phosphorylated ERM were normalized to those for total ERM as a control. Membranes were then incubated with a horseradish peroxidase-conjugated horse anti-rabbit immunoglobulin G antibody (1:5,000). Immunoreactivity was detected by enhanced chemiluminescence autoradiography (ECL Western blotting detection kit; Amersham Pharmacia Biotechnology, United Kingdom).

The obtained samples were washed with ice-cold Tris-HCl buffer (pH 7.4), mixed with the sample buffer (4% sodium lauryl sulfate, 12% beta-mercaptoethanol, and 20% glycerol in 100 mM Tris-HCl [pH 6.8]), sonicated (1 min), boiled (3 min), and finally centrifuged (10,000 g, 60 min, 4°C). The resultant supernatant was stored at −80°C until use. The separation of proteins was carried out according to the previous study (18), with a minor modification. The relative intensity of immunoreactive bands was quantified by Image Master 1D Elite software (Amersham Biotech, Buckinghamshire, United Kingdom), and the data were estimated as percentage of each control.

Experimental protocols. After the surgical procedure and instrumentation, at least 30 min were allowed for stabilization while hemodynamic variables were monitored. The following protocols were examined.

1. We infused graded doses of hydroxyfasudil (10, 30, and 100 μg/kg, IC), and coronary vascular responses were

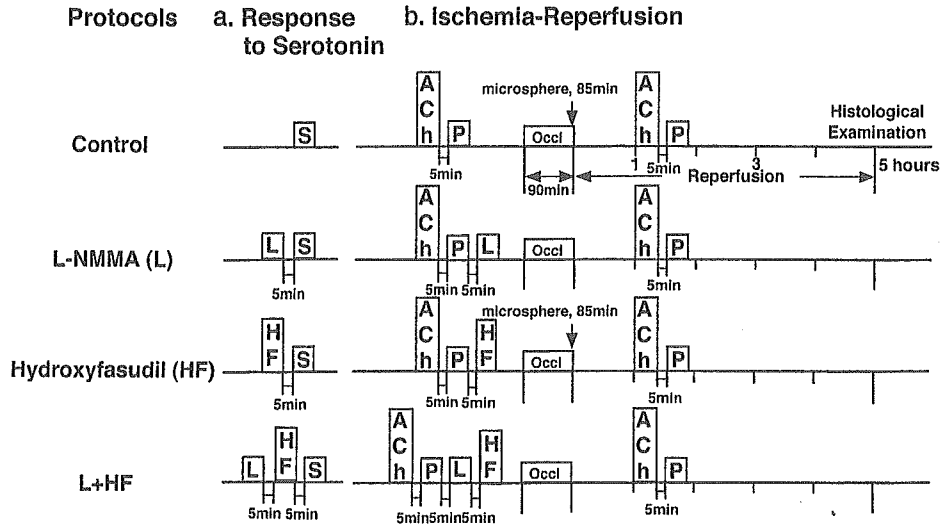

Figure 1. Experimental protocol. S = serotonin; L = L-NMMA; HF = hydroxyfasudil; Ach = acetylcholine; P = papaverine; Occl = coronary occlusion.

analyzed for 4 min by measuring end-diastolic vascular diameters and flows of the LAD.

2. The arteriolar vasoconstrictor response to serotonin before and after hydroxyfasudil (100 μg/kg, IC) was examined with or without inhibition of NO synthase (L-NMMA, 2 μmol/min for 20 min, IC) (Fig. 1). Hydroxyfasudil or L-NMMA was administered at 5 min before infusion of serotonin. The time interval between L-NMMA and hydroxyfasudil was also 5 min.
3. The arteriolar vasodilator responses to endothelium-dependent (acetylcholine, 1 μg/kg IC) and -independent (papaverine, 1 mg IC) vasodilators were examined before and after coronary I (90 min)/R (60 min) under the following four conditions separately in different animals: 1) control conditions, 2) L-NMMA alone, 3) hydroxyfasudil alone (100 μg/kg IC), and 4) hydroxyfasudil plus L-NMMA (Fig. 1). The time interval between each treatment was also 5 min. The basal coronary diameter is before administration of acetylcholine or papaverine either before or after I/R. Hydroxyfasudil and L-NMMA were administered at 5 min after administration of acetylcholine or papaverine. Microspheres were administered at 85 min after the onset of coronary occlusion.
4. After 5 h of reperfusion, LAD and the left circumflex artery (LCX) and myocardial tissue of LAD and LCX area were obtained for Western blotting. We reoccluded the LAD and injected Evans blue dye into a systemic vein. Then myocardial slices (5 mm) were incubated in 1% 2,3,5-triphenyltetrazolium chloride (Sigma, Japan) solution to detect the infarct area. Infarct size was expressed as percentage of the infarct area that was contiguous with area at risk (19).

Drugs. We used the following drugs: hydroxyfasudil (Asahi Kasei Pharma, Tokyo, Japan), acetylcholine (Daiichi-Seiyaku, Tokyo, Japan), papaverine (Dainihon-Seiyaku, Tokyo, Japan), and N^G-methyl-L-arginine (L-

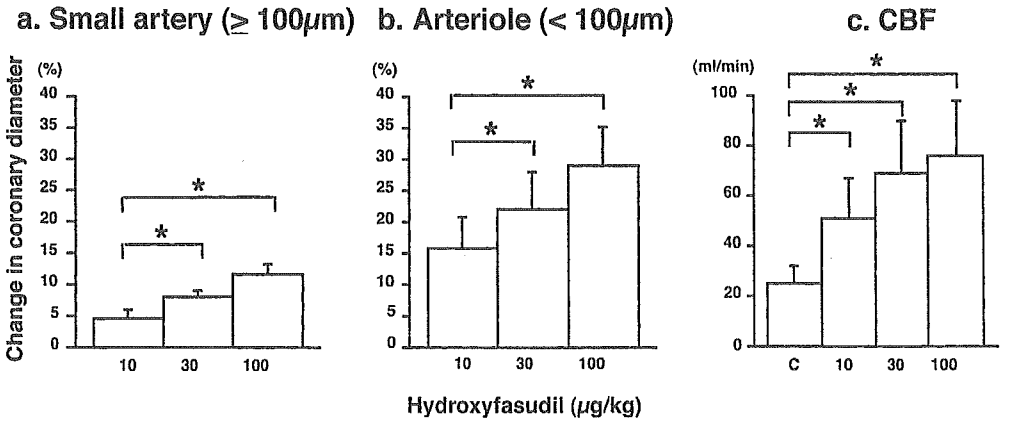

Figure 2. Coronary vasodilator effects of hydroxyfasudil in dogs in vivo. Hydroxyfasudil (10, 30, and 100 μg/kg, IC) caused coronary vasodilation, in a dose-dependent manner, under normal conditions in both small arteries (**a**) and arterioles (**b**). Number of vessels per animal used was 5/3 in small arteries and 7/4 in arterioles, respectively. Hydroxyfasudil also increased coronary blood flow (CBF) in a dose-dependent manner (**c**). *$p < 0.05$.

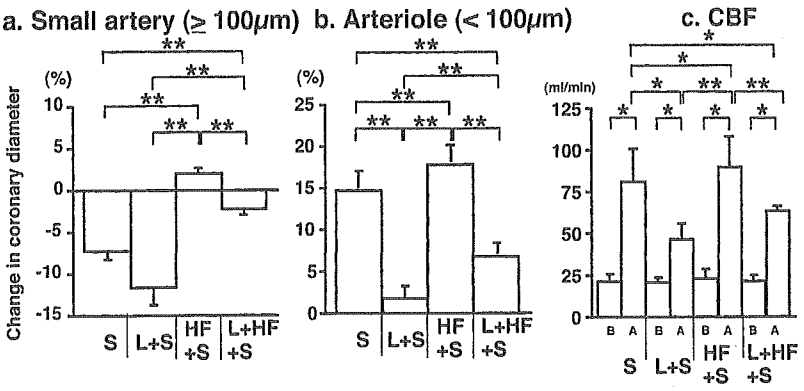

Figure 3. Effects of hydroxyfasudil on serotonin-induced coronary vascular responses in dogs in vivo. Hydroxyfasudil converted the serotonin-induced vasoconstriction of small arteries to vasodilation **(a)** and significantly enhanced the serotonin-induced vasodilation of arterioles **(b)**. L-NMMA significantly attenuated the serotonin-induced vasodilation, which was counteracted by hydroxyfasudil. Number of vessels per animal used was 18/6 for S, L + S and HF + S, 13/4 for L + HF + S. *$p < 0.05$, **$p < 0.01$. S = serotonin; L = L-NMMA; HF = hydroxyfasudil; B = before drug; A = after drug.

NMMA, Sigma). All drugs were diluted in a physiologic saline immediately before use.

Statistical analysis. Results are expressed as means ± SEM. Vascular responses (Figs. 2a to 2c, 3c, 4c, 6c, 7a to 7c, 8a) were analyzed by one-way analysis of variance followed by Scheffe's post-hoc test for multiple comparisons. Difference in the effects of serotonin, acetylcholine, and papaverine on subepicardial microvessels before and after I/R (Figs. 3a, 3b, 4a, 4b, 5a to 5d, 6a, and 6b), and difference between infarct size/risk area and transmural collateral flow with or without hydroxyfasudil (Fig. 8b) were examined by a multiple regression analysis using a model in which the change in coronary diameter was set as a dependent variable (y) and vascular size as an explanatory variable (x) while the statuses of hydroxyfasudil and hydroxyfasudil plus L-NMMA were set as dummy variables (D_1, D_2) in the following equation; $y = a_0 + a_1x + a_2D_1 + a_3D_2$, where a_0 through a_3 are partial regression coefficients. The criterion for statistical significance was at $p < 0.05$.

RESULTS

Coronary vasodilator effects of hydroxyfasudil. Intracoronary administration of hydroxyfasudil caused a significant coronary vasodilation of both small arteries and arterioles (Figs. 2a and 2b, both $p < 0.05$, 10 μg/kg vs. 30 and 100 μg/kg) in a dose-dependent manner under control conditions with a resultant increase in CBF (Fig. 2c, $p < 0.05$, C vs. 10, 30 and 100 μg/kg). Intracoronary hydroxyfasudil did not significantly alter mean aortic pressure or heart rate (Table 1).

Hemodynamics and blood gases during I/R injury. In each experimental condition, mean aortic pressure and heart rate at baseline were constant and comparable (Table 1), and oxygen partial pressure (Po_2), carbon dioxide partial pressure (Pco_2), and pH were maintained within the physiologic ranges (pH 7.35 to 7.45, Pco_2 25 to 40 mm Hg, Po_2 >70 mm Hg) throughout the experiments. Hemodynamic

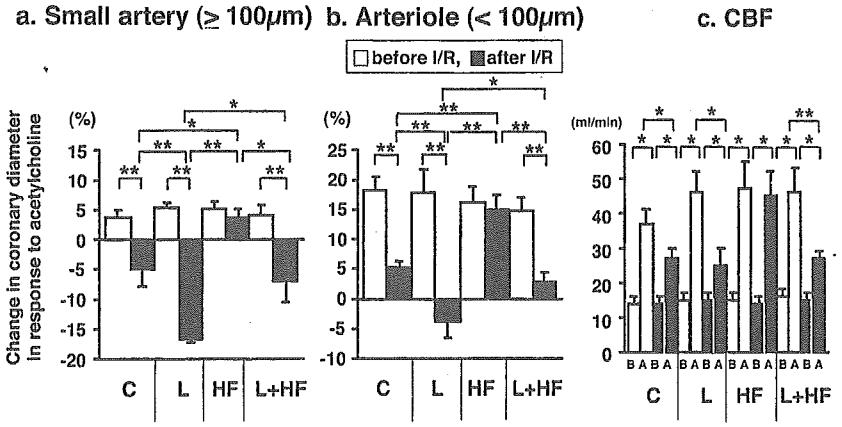

Figure 4. Endothelium-dependent coronary vasodilation before and after coronary ischemia/reperfusion (I/R) injury in dogs in vivo. Coronary I/R significantly impaired coronary vasodilation to acetylcholine under control conditions (C) and L-NMMA (L) further suppressed the vasodilation, whereas hydroxyfasudil (HF) completely preserved the responses. The vasoconstriction induced by L-NMMA after I/R was significantly improved by hydroxyfasudil in small arteries. Hydroxyfasudil also prevented the decrease in coronary blood flow (CBF) after I/R, which effect was attenuated by L-NMMA. Number of vessels per animals used was 7/6 for control (mean diameter 120 ± 7 μm), 5/4 for L-NMMA (123 ± 8 μm), 6/4 for hydroxyfasudil (118 ± 8 μm), and 5/4 for hydroxyfasudil plus L-NMMA (125 ± 9 μm) in small arteries, and 12/6 for control (70 ± 6 μm), 8/4 for L-NMMA (69 ± 7 μm), 8/5 for hydroxyfasudil (68 ± 7 μm), and 11/6 for hydroxyfasudil plus L-NMMA (71 ± 5 μm) in arterioles. I/R = ischemia/reperfusion; B = before acetylcholine; A = after acetylcholine. *$p < 0.05$; **$p < 0.01$.